Global and Planetary Change 171 (2018) 48–64

Contents lists available at ScienceDirect

Global and Planetary Change

journal homepage: www.elsevier.com/locate/gloplacha

# Subsurface temperature model of the Hungarian part of the Pannonian Basin

Eszter Békési[a,*], László Lenkey[b], Jon Limberger[a], Kristóf Porkoláb[a], Attila Balázs[a], Damien Bonté[a], Mark Vrijlandt[d], Ferenc Horváth[b,c], Sierd Cloetingh[a], Jan-Diederik van Wees[a,d]

[a] Department of Earth Sciences, Utrecht University, Budapestlaan 4, Utrecht 3584 CD, Netherlands
[b] Department of Geophysics and Space Science, Eötvös Loránd University, Pázmány Péter sétány 1/c, Budapest 1117, Hungary
[c] Geomega Ltd, Zsil u. 1, Budapest 1093, Hungary
[d] TNO Utrecht, Princetonlaan 6, Utrecht 3584 CB, Netherlands

## ABSTRACT

Hungary is one of the most suitable countries in Europe for geothermal development, as a result of large amounts of Miocene extension and associated thermal attenuation of the lithosphere. For geothermal exploration, it is crucial to have an insight into the subsurface temperature distribution.

A new thermal model of Hungary is presented extending from the surface down to the lithosphere-asthenosphere boundary (LAB) based on a new stochastic thermal modeling workflow. The model solves the heat equation in steady-state, assuming conduction as the main heat transfer mechanism. At the top and the base, we adopt a constant surface temperature and basal heat flow condition. For the calibration of the model, temperature measurements were collected from the Geothermal Database of Hungary. The model is built up in a layered structure, where each layer has its own thermal properties. The prior thermal properties and basal condition of the model are updated through the ensemble smoother with multiple data assimilation technique.

The prior model shows a misfit with the observed temperatures, which is explained fundamentally by transient thermal effects and non-conductive heat transfer. Other misfits can be attributed to a-priori assumptions on thermal properties, boundary conditions, and uncertainty in the model geometry. The updated models considerably improve the prior model, showing a better fit with measured records. The updated models are capable to reproduce the thermal effect of lithospheric extension and the sedimentary infill of the Pannonian Basin. Results indicate that the hottest areas below 3 km are linked to the basement highs surrounded by deep sub-basins of the Great Hungarian Plain. Our models provide an indication on the potential sites for future EGS in Hungary and can serve as an input for geothermal resource assessment.

## 1. Introduction

The Pannonian Basin is one of the most suitable areas for geothermal development in Europe (e.g. Cloetingh et al., 2010; Limberger et al., 2014; Horváth et al., 2015) due to the elevated geothermal gradient and high heat flow density values (Lenkey et al., 2002). The temperature gradient varies between 40 and 50 K/km in the upper 5 km, resulting in elevated temperatures at shallow depth. The 200 °C isotherm can be reached above 4 km, ensuring favourable conditions for deep geothermal exploration. The geothermal prospectivity is largely due to Miocene extension, which resulted in the high thermal attenuation of the lithosphere (Horváth, 1993). The *syn*-rift phase was followed by thermal subsidence and continuous sedimentation, and the basin was finally filled by sediments up to 6–7 km thickness. The porous basin infill and fractured carbonatic rocks are of great interest for geothermal utilization. Thermal water production in the Pannonian Basin has been carried out since the 19th century. On the other hand, fractured crystalline basement rocks are also considered as high potential targets for deep geothermal development (Dövényi et al., 2005), but production from these high-temperature high-pressure systems has not taken place yet.

The main controlling parameters of geothermal systems are the flow rate and the temperature of the reservoir fluid. The minimum production temperatures required for district heating and electricity are 70 °C and 130 °C respectively, but the exact temperature ranges vary due to the geothermal power plant configurations. Since the flow rate is strongly dependent on the permeability of the reservoir, in most cases treatment to enhance the permeability is necessary for geothermal power generation. High temperature basement rocks at relatively shallow depth are considered one of the most promising targets for Enhanced Geothermal Systems (EGS) due to the reduced costs of drilling and higher natural permeability. Therefore, to find the location of

* Corresponding author.
*E-mail address:* e.bekesi@uu.nl (E. Békési).

http://dx.doi.org/10.1016/j.gloplacha.2017.09.020
Received 23 June 2017; Received in revised form 29 September 2017; Accepted 29 September 2017
Available online 30 September 2017
0921-8181/ 

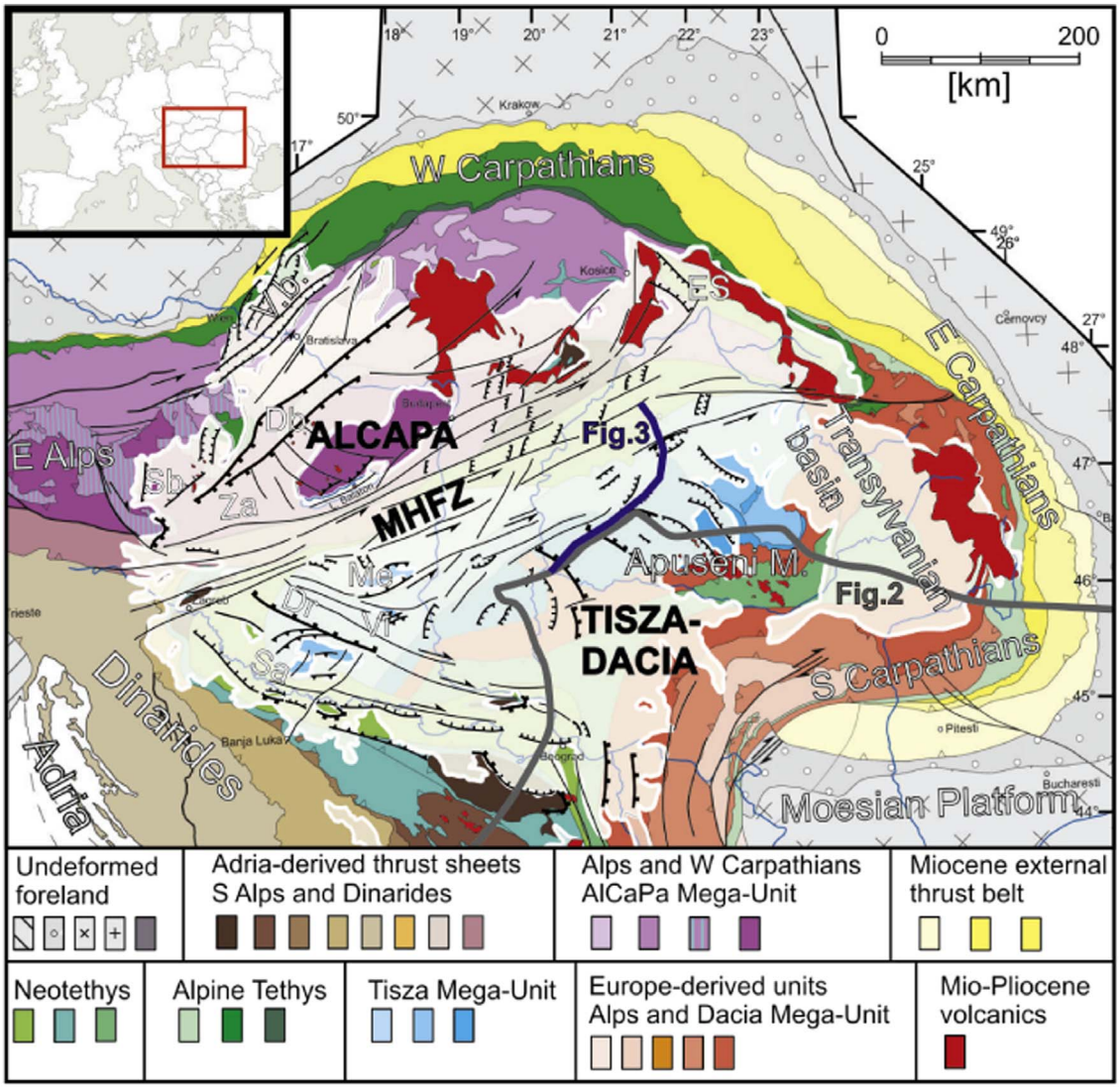


**Fig. 1.** Miocene–Quaternary tectonic map of the Pannonian Basin showing the present-day extent of the Neogene sediment cover of the Pannonian, Vienna, and Transylvanian basins and the major Miocene to Quaternary faults after Balázs et al. (2016). Vb = Vienna Basin, Sb = Styrian basin, Dr = Dráva sub-basin, Sa = Sava sub-basin, Za = Zala sub-basin, Me = Mecsek hill, Vi = Villány mountains, Db = Danube basin, ES = East Slovakian basin, MHFZ = Mid-Hungarian Fault Zone.

these reservoirs, it is crucial to have a good constraint on the subsurface temperature distribution.

Several studies on the heat flow density and subsurface temperature field of the Pannonian Basin have been performed. Čermák and Bodri (1986) calculated the temperature distribution in steady-state along regional deep seismic sections and found that the high heat flow in the Pannonian Basin originated from the mantle. Subsurface temperatures and the integrated strength in the lithosphere were calculated along two cross sections through the Western Carpathians – Pannonian Basin – Transylvanian basin – Eastern Carpathians by Lankreijer et al. (1999). They concluded that the internal part is characterized by hot and weak lithosphere, whereas the European foreland and Ukrainian Shield comprise the mechanically strong frame of the Carpathians. Lenkey (1999) corrected the surface heat flow density for the cooling effect of Neogene and Quaternary sedimentation by time-dependent thermal modeling. The subsurface temperature distribution of Hungary was constrained by Dövényi et al. (2005). They found that the most suitable areas for EGS plants are the basement highs of the Great Hungarian Plain. The geothermal resources of Hungary were evaluated in several earlier studies (e.g. Rezessy et al., 2005; Horváth et al., 2015). Lenkey et al. (2017) constructed both a steady-state and a time-dependent 3D lithospheric-scale thermal model of the Alpine-Pannonian transition zone.

In this paper we present the first 3D lithospheric-scale high-resolution thermal model of Hungary. Subsurface temperatures are shown for different depth intervals providing an insight into deep temperature anomalies. Therefore, our model can serve as a reference model to reveal potential areas for geothermal development in Hungary. Additionally, our model predicts subsurface temperature in larger depth, which is crucial to understand the thermo-mechanical state of the lithosphere (Cloetingh et al., 2010).

## 2. Formation and evolution of the Pannonian Basin

The Neogene formation of the Pannonian Basin by extension was preceded by Cretaceous-Paleogene contraction and nappe stacking in the Circum-Pannonian region. The former orogenic area now constitutes the basement of the Pannonian Basin and consists of two major structural units: the AlCaPa and the Dacia-Tisza mega-units (Fig. 1). The evolution of these units reflects the opening and subsequent closure of the Neotethys and Alpine Tethys oceanic realms. (e.g. Csontos and Vörös, 2004; Schmid et al., 2008). The AlCaPa Mega-unit is an Adria-

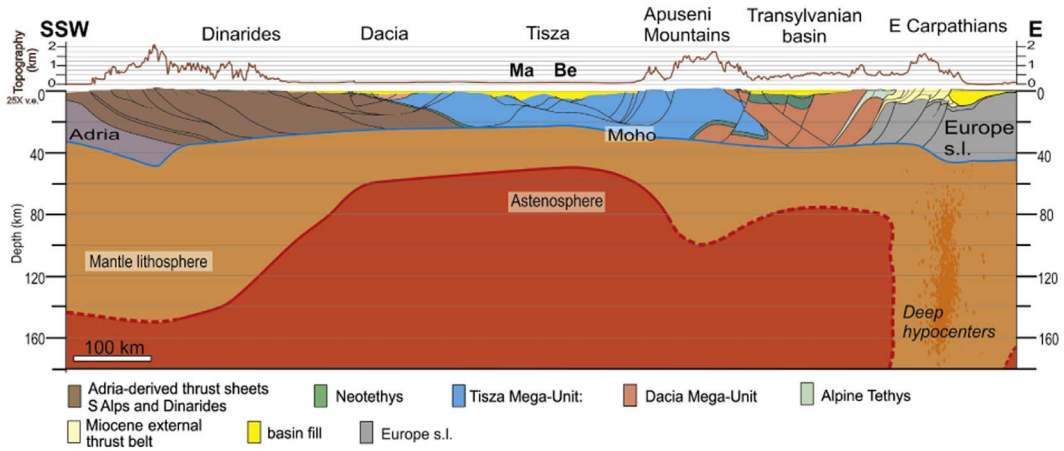


**Fig. 2.** Lithospheric-scale cross-section over the Dinarides–Pannonian Basin–Apuseni Mountains–Transylvanian Basin–East Carpathians after Balázs et al. (2017) (see for location Fig.1). Ma – Makó sub-basin, Be – Békés sub-basin.

derived composite thrust sheet that was sutured to Europe as a result of the Cretaceous-Paleogene closure of the Alpine Tethys realm. The shortening and nappe stacking was followed by lateral extrusion in the AlCaPa due to the combination of overthickening in the Alps and the initiation of slab-rollback in the Carpathians (Ratschbacher et al., 1991). The Tisza-Dacia mega-unit was emplaced on top of the Dinaridic nappes by the final closure of the Neotethys during latest Cretaceous to Paleogene times. Onset of Oligocene-Early Miocene extrusion was accompanied by large-scale offsets along transcurrent shear zones and opposite sense rotations, i.e., counterclockwise in AlCaPa and clockwise in Tisza-Dacia (Balla, 1986; Balla, 1988; Márton and Fodor, 2003). These mega-units were juxtaposed along a major suture zone, the Mid-Hungarian Fault Zone (MHFZ) that accommodated the former subduction polarity change of the Alpine- and Neotethys (Csontos and Nagymarosy, 1998).

Similar to other Mediterranean back-arc basins (e.g. Faccenna et al., 2014) extensional deformation was localized at inherited weakness zones, which led to asymmetric basin evolution (Fig. 2; Balázs et al., 2017) and reactivated former thrust and nappe contacts (e.g. Horváth and Rumpler, 1984; Tari et al., 1992). This controlled the extensional exhumation of deep crustal rocks and the formation of metamorphic core complexes at the Alpine and Dinaridic basin margins (e.g. Tari et al., 1992; Fodor et al., 2008; Ustaszewski et al., 2010; Matenco et al., 2016). Initial pulses of back-arc extension were followed by the progressive opening of deep half-grabens between Early to Late Miocene (Merten et al., 2010; Matenco and Radivojević, 2012). The lithospheric structure and the geometry of the basin system is shown in Fig. 2. The sub-basins are characterized by different timing of active extensional deformation and sedimentation, recorded by the *syn*-kinematic basin fill, proving that extension in the Pannonian basin migrated in space and time throughout the entire Miocene in the basin (Fig. 3; Balázs et al., 2016).

The sedimentary fill of the Pannonian Basin reflects the migration of extensional deformation and subsidence in time and space as well as the closure and re-opening of oceanic gateways, which happened repeatedly starting during Late Eocene in the Paratethys region due to uplift of orogens surrounding the basin system. The closure of oceanic gateways resulted in a marine to brackish lacustrine environment in the Pannonian Basin characterized by an endemic fauna which required the establishment of a separate regional biostratigraphy in the Central Paratethys region (e.g. Báldi and Royden, 1986; Nagymarosy and Muller, 1988).

Early Miocene sedimentation was characterized by shallow marine deposits in the northwestern part of the Pannonian Basin (Hámor, 2001), contrasting the fluvial and lacustrine environment in the area of the Great Hungarian Plain (e.g. Pavelić et al., 2001). Continuous extension resulted in the deposition of deep basinal Middle Miocene sediments in the depocenters such as grabens and half-grabens (Fig. 3), and near-shore shallow marine siliciclastic and carbonatic deposits along the uplifted footwalls of active normal faults.

Active extension was followed by post-rift thermal subsidence and basin inversion. The onset of post-extensional evolution in the Pannonian Basin appears to be older in the western parts and younger towards the SE Carpathians (Figs. 1, 3). In the NW part of the basin system, significant normal displacements ceased in the Middle Miocene (Tari et al., 1999), while in the Great Hungarian Plain cessation of active extensional deformation occurred during Late Miocene times, for instance in the Makó or Derecske sub-basins (Fig. 3; Balázs et al., 2016).

Post-rift sedimentation took place in a completely restricted lake environment (i.e., Lake Pannon) following the final isolation of the region due to significant uplift in the Carpathians (Magyar et al., 1999). Sedimentation was controlled by a fluvial system which transported large amount of sediments from the neighboring orogenic areas and determined a characteristic pattern of shelf margin and slope progradation towards the deep basin (Pogácsás et al., 1988; Vakarcs et al., 1994; Magyar et al., 2013). Fig. 3 shows the tectono-sedimentary architecture of the post-rift basin fill; coeval but lithologically different sediments deposited in the confines of the progradational system: alluvial plain, delta, prograding shelf slope, turbiditic, and deep hemipelagic formations characterize the post-rift strata (e.g. Juhász, 1991). The thick post-rift siliciclastic deposits (up to 7 km beneath the Great Hungarian Plain) essentially determine the present hydraulic and thermal characteristics of the Pannonian Basin, and are discussed below in details.

The Neogene-Quaternary formation of the Pannonian basin was accompanied by diverse magmatism. Different stages of silicic, calc-alkaline, and alkaline basaltic volcanic activity were largely controlled by the lithospheric extension in the Pannonian basin and the dehydration of the subducting slab beneath the Carpathians (e.g. Kovács et al., 2004; Harangi and Lenkey, 2007).

Continuous push of the Adriatic microplate towards the thermally weakened Pannonian Basin combined with the cessation of slab-rollback process beneath the Carpathians resulted in Late Miocene to recent basin inversion marked by newly formed reverse faults, reactivated structures, and basin-scale folding effects (e.g. Horváth and Cloetingh, 1996; Fodor et al., 2005; Bada et al., 2007; Magyar and Sztanó, 2008).

## 3. Temperature and heat flow data

We calibrated our models with subsurface temperature and heat flow data obtained from the Geothermal Database of Hungary (Dövényi and Horváth, 1988; Fig. 4; Dövényi et al., 2002). The dataset is based

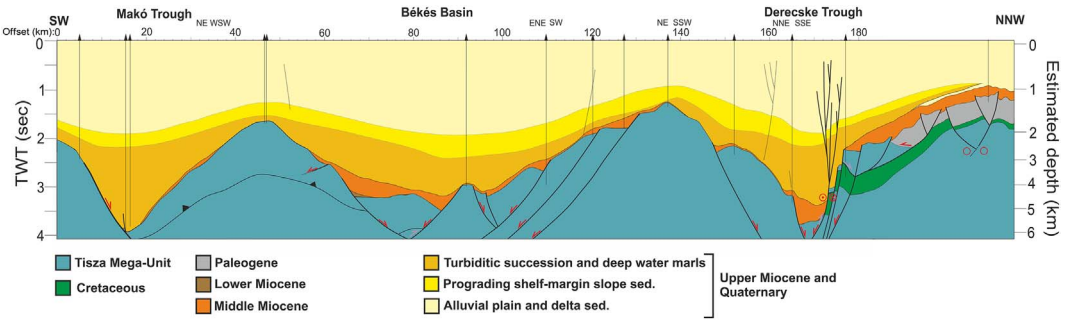


**Fig. 3.** Interpreted composite reflection seismic transect from the eastern part of the Pannonian Basin simplified after Balázs et al. (2016) showing the main tectonic and stratigraphic features of the area (see for location Fig. 1).

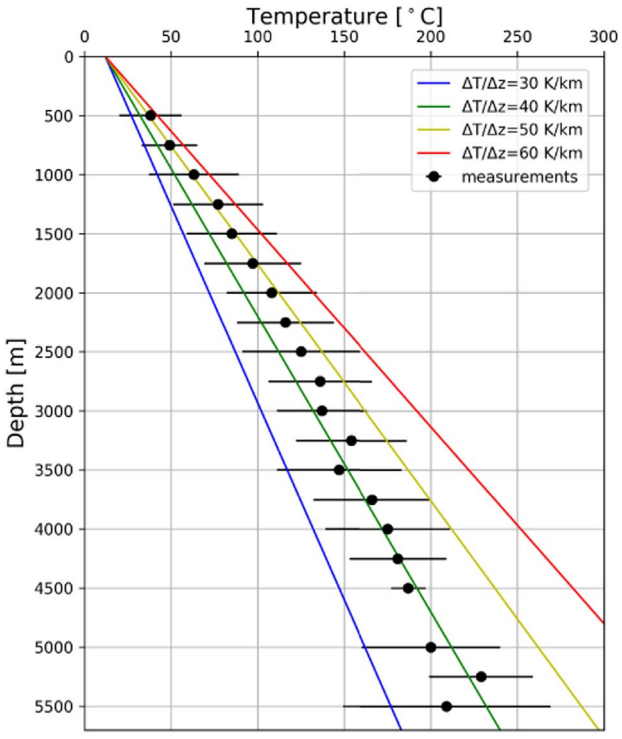


**Fig. 4.** Characteristic temperature-depth profile from the Pannonian Basin modified after Dövényi and Horváth (1988). The circles and bars indicate the average value and variation of temperature measurements at certain depth (respectively). The lines represent geotherms corresponding to 30, 40, 50 and 60 K/km.

on Bottom Hole Temperature (BHT) measurements, inflowing and outflowing water temperatures, Drill-Stem Tests (DST) in hydrocarbon wells and steady-state temperature measurements from about 4800 boreholes.

Primary heat flow determinations are available from 28 boreholes in the central part of the Pannonian Basin with reliable temperature data at different depths and thermal conductivity measurements on core samples. Furthermore, heat flow was calculated in boreholes where the lithology and reliable temperature data were available using conductivity versus depth diagrams after (Dövényi and Horváth, 1988). The observed heat flow may be disturbed by fast sedimentation, erosion and groundwater flow. Heat flow determinations were corrected for the thermal effect of sedimentation taking into account the variation in sedimentation rate and change in the thermal properties due to compaction (Lenkey, 1999).

Fig. 5 shows the corrected surface heat flow map of the Pannonian Basin and its surroundings (Lenkey et al., 2002). Heat flow values are in the range of 50 to 130 mW/m$^2$ with a mean of 100 mW/m$^2$. In general, the Pannonian Basin is characterized by considerably higher heat flow than the surrounding areas. The Ukrainien and Moesian Platforms exhibit low heat flow (40–50 mW/m$^2$). Extremely low values (30 mW/m$^2$) in the Outher Dinarides can be explained by the cooling effect of descending water flow in the karstified carbonatic rocks (Ravnik et al., 1995). The Carpathians, Inner Dinarides and Bohemian Massif are marked by average continental heat flow around 50–70 mW/m$^2$. The average heat flow density in the Vienna basin is 50–70 mW/m$^2$, whereas the Danube basin exhibits elevated values (80–90 mW/m$^2$). The Transylvanian basin is considerably colder than the central basins, reflecting the differences in the mechanisms of basin evolution (e.g. Tiliţă et al., 2013). In the southern part of the Eastern Carpathians the heat flow is considerably higher related to recent volcanic activity (e.g. Karátson et al., 2013; Szabó et al., 1992). Heat flow density in the inner part of the Pannonian Basin shows a NW to SE trending pattern, with elevated values towards the SE. Surface heat flow in the Styrian basin and Zala-Mura basin is around 90 and 110 mW/m$^2$, respectively. Values in the southern, eastern (Great Hungarian Plain and its continuation into the Serbian basin and Vardar zone) and in the northeastern (Eastern Slovakian basin) part of the Pannonian Basin exceed 110 mW/m$^2$, forming the hottest areas of the region. On the other hand, lower heat flow in the Makó trough and Békés sub-basin can be explained by the cooling effect of the ca. 7–8 km thick young sediments (Lenkey, 1999). A significantly large heat flow anomaly can be attributed to the Serbian basin, which conforms well with the low crustal and lithospheric thickness of the region (Fig. 2). The Transdanubian Range and some parts of the Hungarian mountains in the Northeast built up by fractured and karstified carbonates are characterized by low heat flow (50 mW/m$^2$), due to the infiltration of cold meteoric water. Descending water penetrating deep into the carbonates is heated up and may return to the surface along faults at hot springs near the foot of the mountains. Lenkey et al. (2002) has calculated the convective heat flow component caused by groundwater flow in recharge areas from the ratio of the total energy output and the area of the mountains. Results show that the heat flow corrected for convective effects is close to the heat flow observed around the exposed carbonates.

## 4. Hydraulic systems and geothermal resources

Two regional water flow systems exist in the Pannonian Basin representing an upper and lower domain (Tóth and Almási, 2001). The upper domain is characterized by gravity-driven flows directed downwards in recharge areas and upwards in discharge areas. These systems prevail both in porous Neogene and Quaternary sedimentary rocks and exposed Mesozoic carbonates together with their subsurface continuations. The subsurface extent of gravity-driven flows are mostly about 2 km in the basin infill, while flows can penetrate deeper in the permeable carbonates (Horváth et al., 2015). In the lower hydraulic domain an overpressure-driven flow system prevails in the Early and Middle Miocene synrift sediments and fractured pre-Cenozoic basement rocks. Lower Pannonian sediments (mainly marls, based on the regional stratigraphic subdivision (e. g. Piller et al., 2007)) form the upper lid of

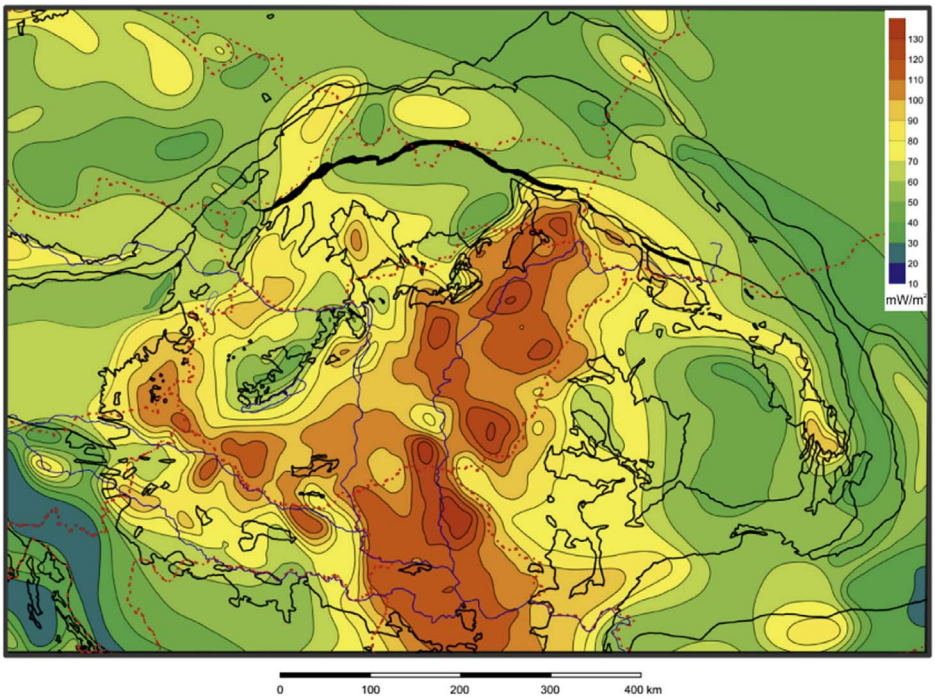


**Fig. 5.** Surface heat flow map corrected for sediment blanketing effects of the Pannonian Basin and its surroundings after Lenkey et al. (2002) modified in the Eastern Alps after Hofmann and Schönlaub (2007).

these systems. The upper and lower domains are separated by a pressure seal, but these systems are not completely isolated, since hydraulic communication between the different parts of the flow domains may exists along open faults (e.g. Mádl-Szőnyi and Tóth, 2009; Mádl-Szőnyi et al., 2017).

The porous basin infill is made up of mainly sand and sandy clay layers representing shelf front, shelf, and alluvial plain deposits that form the largest hydrostratigraphic unit in the Pannonian Basin. In general, gravity-driven fluid flow systems are directed from the peripheral areas towards the central part of the Pannonian Basin. In the Great Hungarian Plain - where the relief is very smooth - local flow systems with shallow streamlines follow the local topographic variations. Additionally, the major recharge and discharge areas are connected by deeper penetrating streamlines. Gravity-driven flow systems in the Upper Pannonian (based on the regional stratigraphic subdivision (e. g. Piller et al., 2007)) geothermal aquifers in the western part of Hungary are strongly connected to the Austrian, Slovenian and Slovakian aquifers (Tóth et al., 2016).

Fractured and karstified Mesozoic carbonates representing upper nappes in the AlCaPa Mega-unit (e.g. Transdanubian Range) and Tisza-Dacia Mega-unit (e.g. Mecsek, Villány-Bihor, Békés-Codru nappes) and Dinaric units (e.g. below the Mid-Hungarian Fault Zone or Bükk) also exhibit considerable water resources (Fig. 6). As discussed in the previous section, gravity-driven fluid flow systems cause a reduction of heat flow of large carbonate plateaus resulting in lower temperatures due to descending cold water (Fig. 7). The penetration depth of streamlines can be approximated by the temperature of hot springs at discharge areas, suggesting that water even emerges from 3 km depth (Lenkey et al., 2002). Water circulation is mainly driven by the hydraulic head, but ascent of hot water is also enhanced by temperature-induced density and viscosity reduction (Goldscheider et al., 2010). Considerable amount of hot springs are located along fault zones, for instance, in Budapest and Hévíz (Fig. 6), located East and West of the Transdanubian Range, respectively.

It has been shown by Gordon and Flemings (1998) that overpressured hydrostratigraphic units are commonly observed in sedimentary basins with ongoing subsidence and sedimentation. This phenomena is also present in the deeper parts of the Pannonian Basin. In the fractured Mesozoic basement rocks, free convection systems can occur due to the high permeability, temperature and pressure (Lenkey et al., 2002). These systems are well-known from Fábiánsebestyén (Fig. 6), where a dramatic blowout occurred in drilling the Triassic carbonates of the Villány-Bihor basement unit.

Neogene to Quaternary clastic basin infill, Mesozoic carbonates and the fractured crystalline basement represent the main potential target zones for geothermal utilization in Hungary. The thermal water production rate from the porous Pannonian beds is typically 200–300 $m^3$/day with the production temperature in the range of 30–100 °C. Flow rates of geothermal wells drilled into fractured Mesozoic rocks reach even 1000–1500 $m^3$/day due to their considerable subsurface extent and high permeability (Horváth et al., 2015), with production temperatures even above 150 °C (Rotár-Szalkai et al., 2017). Fractured crystalline basement rocks at larger depth are also high potential targets for deep geothermal development (Dövényi et al., 2005). However, production from these high-temperature high-pressure systems has not been carried out yet.

## 5. Methodology

We first adopt an a priori physics-based forward model in order to construct the thermal model of the deep subsurface of Hungary. Then, the prior parameterization of the model is updated through a data assimilation method in order to provide predicted temperatures to fit better with the observations (Fig. 8). Subsurface temperatures are obtained by solving the heat equation in steady-state, assuming conduction as the main heat transfer mechanism. Initial calculations are performed in a multi-1D approach and are incorporated in the 3D forward model as initial information on the temperature and thermal properties in each of the grid cells. The 3D forward model solves the heat transport equation by a finite-difference approximation using the Preconditioned Conjugate Gradient method (PCG). A variation in the basal condition (temperature or heat flow), radiogenic heat generation and the vertical thermal conductivity can be introduced through the ensemble smoother with multiple data assimilation technique (ES-MDA, Emerick and Reynolds, 2013) to obtain a better fit with observed temperatures, described in Section 5.5. The ES-MDA has also been applied by Fokker et al. (2016) for reservoir modeling to constrain subsurface model parameters. More details on the methodology can be found in the

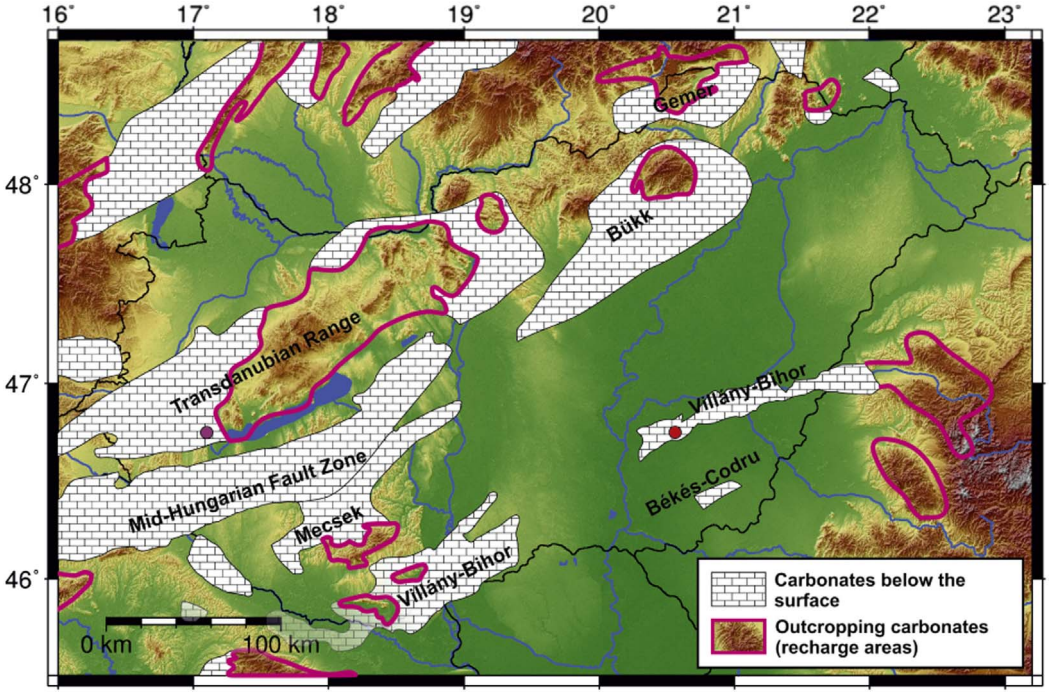


**Fig. 6.** Map showing the outcropping fractured-karstified Mesozoic carbonates (recharge areas) and their subsurface extent (discharge areas) modified after Horváth et al. (2015). Purple and red dots indicate Hévíz and Fábiánsebestyén, where hydrothermal convection due to gravity-driven flow systems and overpressured systems occur, respectively.

IMAGE-D6.01 report (http://www.image-fp7.eu/reference-documents/Pages/default.aspx) and Limberger et al. (this volume).

### 5.1. Geometry of the model

The thermal model was built in the Hungarian National Coordinate System (EOV) extending vertically from the surface until the litosphere-astenosphere boundary (LAB). The outline of the model is identical with the political boundary of Hungary. Subsurface temperatures were calculated through a regular 3D grid with a horizontal resolution of 2.5 km, a vertical resolution of 200 m for the uppermost 7 km, and 3 km down to the depth of the LAB. The geometry of the model is outlined by 9 layers: 6 sedimentary layers, upper crust, lower crust and lithospheric mantle, where each layer is described by its own material properties. The crustal and lithospheric thickness are obtained from Horváth et al. (2006), with the average values of 27 km and 60 km, respectively. For the sedimentary layers we follow horizons obtained from the map database of the Geological and Geophysical Institute of Hungary (https://map.mfgi.hu/) following the regional stratigraphic subdivision (e. g. Piller et al., 2007). The basement is defined by the pre-Cenozoic map of Haas et al. (2010) supplemented by the outcropping Mesozoic carbonates and their subsurface extent from Horváth et al. (2015). The division of crystalline and carbonate basement is particularly relevant to account for the contrast between the thermal properties and to model potential hydrothermal convection.

### 5.2. Thermal properties

The thermal conductivity values of the clastic sediments were adopted after (Dövényi and Horváth, 1988) using the porosity-

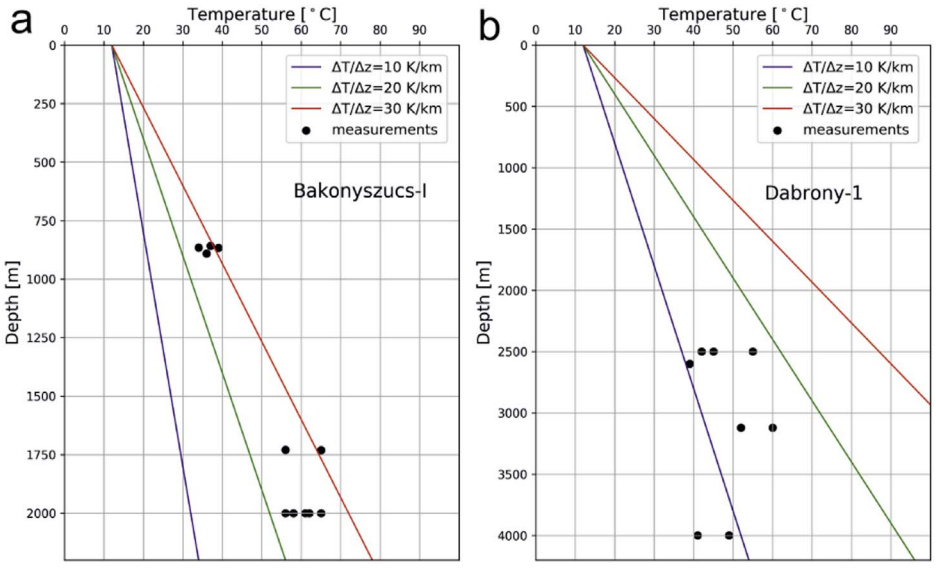


**Fig. 7.** Temperature measurements (black circles) from wells drilled in the recharge area of the Transdanubian Range. The lines represent geotherms corresponding to 10, 20 and 30 K/km. Note the very low observed temperatures due to the infiltration of cold meteoric water.

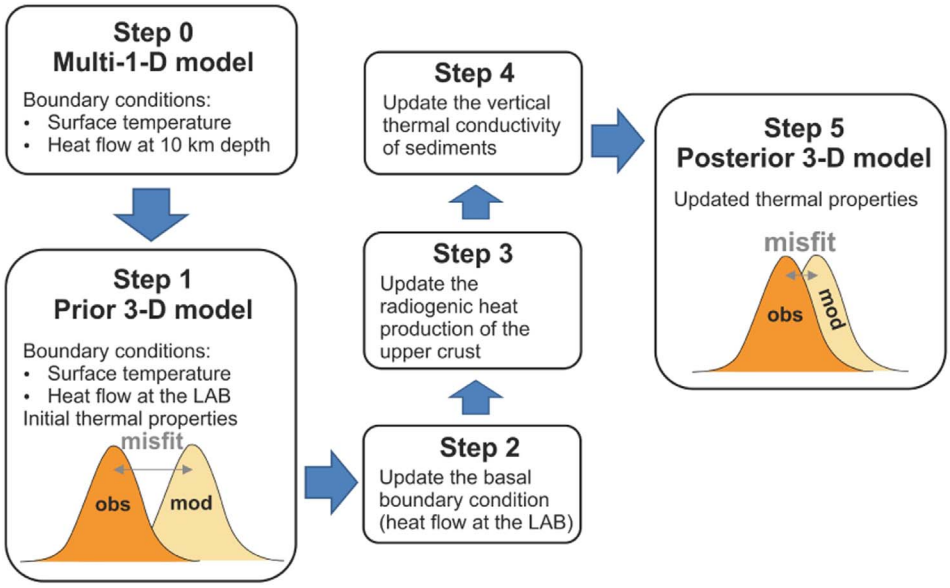


**Fig. 8.** Overview of the modeling workflow.

dependent empirical formulas for sandstones and shales in the Pannonian Basin. The sediments are subdivided into lithotypes, and their thermal properties are represented by a mixture of typical lithologies listed in Table 1. The thermal conductivity of Mesozoic carbonates is defined as a mixture of typical values of limestones and dolomites after Hantschel and Kauerauf (2009). The matrix conductivities of the different sedimentary units were calculated as the arithmetic mean for horizontal conductivities, and harmonic mean for vertical conductivities following the methodology of (Hantschel and Kauerauf, 2009). To calculate the thermal properties of the crust and mantle, we follow the methodology that was applied by Limberger et al. (2017) and reported in Table 2. For the upper and lower crust, we adopted the temperature and pressure dependent function of Chapman (1986). With increasing temperature down to the lithospheric mantle, the contribution of the radiative component of the thermal conductivity increases compared to the lattice component. Therefore, the conductivity of the lithospheric mantle was calculated by taking into account the effect of the radiative component after Schatz and Simmons (1972). For the lattice thermal conductivity of the lithospheric mantle, we follow the formula of Xu et al. (2004).

The radiogenic heat production of each sedimentary unit was selected to constants calculated as a mixture of typical values of sandstones and shales after (Hantschel and Kauerauf, 2009). The volumetric heat production of the upper crust is considerably higher than the sediments and lower crust, since its typical lithotype is granite. In the prior model we set the heat generation of the upper crust to 1.4 $\mu W/m^3$ corresponding to typical continental upper crustal values. The heat production of Neogene volcanic rocks in Hungary is similar in case of basalts and andesites, on the other hand rhyolites and dacites have higher values (Lenkey and Surányi, 2006). For the heat generation of the lower crust and lithospheric mantle, we prescribed 0.5 and 0.02 $\mu W/m^3$ (Hasterok and Chapman, 2011), respectively.

**Table 1**
Overview of the sedimentary layers and their corresponding lithologies.

| Layer name | Lithology | Radiogenic heat production [$\mu W/m^3$] | Thermal conductivity [W/m*K] |
|---|---|---|---|
| Quaternary (Q) | 70% clastic sediment sand<br>30% clastic sediment shale[a] | 1.0 | Bulk values per lithotypes (mixed lithologies), dependent on compaction (Dövényi and Horváth, 1988) |
| Upper-Pannonian (UP) | 50% clastic sediment sand<br>50% clastic sediment shale[a] | 1.2 | |
| Lower-Pannonian (LP) | 10% clastic sediment sand<br>90% clastic sediment shale[a] | 1.6 | |
| Neogene (pre-Pannonian) (N) | 65% clastic sediment sand<br>35% clastic sediment shale[a] | 1.0 | |
| Paleogene (P) | 20% clastic sediment sand<br>80% clastic sediment shale[a] | 1.5 | |
| Mesozoic carbonates (M) | 50% limestone typical<br>50% dolomite typical | 0.5 | Bulk values per lithotypes (mixed lithologies), dependent on compaction and temperature (Hantschel and Kauerauf, 2009) |

[a] Lithological composition of the sedimentary layers were obtained from Berczi (1988).

**Table 2**
Overview of the average thickness, radiogenic heat production values and thermal conductivities of the crust and lithospheric mantle.

| Layer name | Average thickness [km] | Radiogenic heat production [μW/m$^3$] | Thermal conductivity [W/m∗K] |
|---|---|---|---|
| Upper crust (UC) | 27 (crustal thickness) | 1.4 | Pressure- and temperature-dependent (Chapman, 1986) |
| Lower crust (LC) | | 0.4 | Pressure- and temperature-dependent (Chapman, 1986) |
| Lithospheric mantle (LM) | 60 (lithosphere thickness) | 0.02 | Lattice thermal conductivity (Xu et al., 2004) and radiative thermal conductivity (Schatz and Simmons, 1972) |

### 5.3. Boundary conditions

We constructed three models by adopting different basal boundary conditions. Our first and second model are based on surface heat flow observations, whereas the third model accounts for the time-dependent effect of sub-recent lithospheric extension. For the top of all models we prescribed the average surface temperature of 12 °C as a Dirichlet boundary condition. The vertical edges of the models were marked by zero heat flow.

Since the elevated surface heat flow and high geothermal gradient in the Pannonian Basin are due to lithospheric-scale tectonic processes, the thermal effect of extension can only be reproduced by lithospheric-scale modeling. To account for the interplay between deep and surface processes, we have to link our observations near the surface with the thermal anomalies deeper down in the lithosphere. Therefore, we derived the lower boundary condition of our models from the surface heat flow. First, we imposed a Neumann boundary condition on heat flow at 10 km depth for the multi 1D temperature calculations of both models. In Model 1 and Model 2, we opted for a constant value of 70 mW/m$^2$, which was calculated by subtracting the total radiogenic heat production of each vertical column from the surface heat flow after Lenkey et al. (2002) and taking their average value. Heat flow derived from the crustal and subcrustal stretching factors (Fig. 9) after Lenkey (1999) was introduced in the multi-1D calculations as a boundary condition of Model 3 in 10 km depth. Similar to the previous model, tectonic surface heat flow was corrected for the effect of heat generated in rocks until 10 km depth. Heat flow at the LAB derived from the multi 1D models was used as a basal boundary condition for the 3D calculations summarized in Table 3.

It has been shown by Sclater et al. (1980) and Royden et al. (1983) that the high post-rift subsidence rate and the elevated heat flow density of the Pannonian Basin could only be explained if the mantle part of the lithosphere was thinned more than the crust. Therefore, for Model 3, we calculated the surface heat flow from the stretching parameters by assuming instantaneous lithospheric thinning, which has occurred 17 Ma before present. We performed a multi-1D tectonic modeling following the depth-dependent extensional model of Royden and Keen (1980) with the corresponding parameters listed in Table 5. We assumed the original crustal and lithospheric thickness of 30 km and 120 km, respectively. Furthermore, we took into consideration the effect of heat generation in the upper crust (and its reduction due to the thinning of the crust) and the influence of sediment infill on the surface heat flow evolution. The latter is of great importance for fast to moderate sedimentation rates (e.g. Theissen and Rüpke, 2010; Van Wees et al., 2009), which is especially relevant for the southeastern part of the Pannonian Basin. Following Pollack and Chapman (1977) we assumed that the radiogenic heat production rate within the upper crust accounts for 40% of the initial surface heat flow. The lower crustal heat generation was neglected.

### 5.4. Controlling temperatures and data uncertainty

We calibrated the models with temperature measurements from the Hungarian Geothermal Database (Dövényi and Horváth, 1988; Dövényi et al., 2002). Prior to the modeling, measured temperature values were carefully evaluated, and observations with high error were discarded from the dataset. Errors of the remaining data were set in the range of 5 and 20 °C, depending on the quality of the measurement. It is commonly accepted to mark the Drill-Stem Tests (DSTs) and Formation Tests by the uncertainty of ± 5 °C (e.g. Bonté et al., 2012). The uncertainty of the Bottom Hole Temperatures (BHTs) is estimated by lying within a deviation of ± 10 °C (Goutorbe et al., 2007). The remaining measurements were evaluated following the uncertainty given in the database. Since only one observation per grid cell is supported in the calculations, in case of multiple observations, the measurement with lower uncertainty is selected. Finally, the number of temperature measurements used for calibration was 3858. The location of the data points is presented in Fig. 10, and the number of measurements used for calibration between 1 and 6 km depth are reported in Table 4.

To account for the variation of the heat flow in Model 2 without incorporating errors of surface heat flow determination ( ± 10–25%, Lenkey et al., 2002), we sampled the heat flow observations at well locations. Since models can only be calibrated with temperature data (heat flow observations are not supported for calibration), it was necessary to calculate the corresponding temperatures. Resampled surface heat flow values were converted to equivalent temperature values at 400 m depth using the corresponding thermal conductivities of the sedimentary layers as:

$$T_z = \frac{Q_s}{k} z + T_s$$

where $T_z$ is the temperature at z = 400 m, $Q_s$ denotes the surface heat flow, and $T_s$ is the surface temperature. The obtained temperature values were added to the calibration dataset for Model 2.

### 5.5. Ensemble smoother with multiple data assimilation

The prior parameterization of the model is updated trough the data assimilation procedure, adopting measured temperatures as target observations. The goal of the inversion is to find the solution which minimizes the weighted sum of differences with data and with a prior model estimate. In the ensemble smoother (ES), the equation for the assimilated model parameter vector $\boldsymbol{m}^a$ for multiple data assimilation is written as:

$$\boldsymbol{m}_j^a = \boldsymbol{m}_j + \widehat{\boldsymbol{C}}_{md}(\widehat{\boldsymbol{C}}_{dd} + \boldsymbol{C}_d)^{-1}(\boldsymbol{d}_j - \widehat{\boldsymbol{d}}_j)$$

For $j = 1, 2, [\ldots], N_e$, where $N_e$ denotes the number of ensembles (Emerick and Reynolds, 2013). Each ensemble consists of a stochastically sampled model parameter realization, and associated model forecast. $\widehat{\boldsymbol{C}}_{md}$ is the cross-covariance matrix between the prior vector of model parameters, $\boldsymbol{m}$, and the vector of predicted data, $\boldsymbol{d}$. $\widehat{\boldsymbol{C}}_{dd}$ denotes the $N_d \times N_d$ auto-covariance matrix of predicted data, where $N_d$ represents the number of measurements. $\boldsymbol{C}_d$ is the $N_d \times N_d$ covariance matrix of observed data measurement errors. $\widehat{\boldsymbol{d}}_j$ denotes forecasted values by the thermal model at the observation points. $\boldsymbol{d}_j = \boldsymbol{d}_{obs} + \epsilon_j$, where $\boldsymbol{d}_{obs}$ is the data vector, and $\epsilon$ denotes the data error vector.

Basically, an ensemble of solutions is produced, each consistent with the prior statistics. The mean of the ensemble is taken as the best guess, and the error-covariance of the updated model ensemble is calculated from the ensemble anomalies. If the relationship between the parameters and the forecast is linear, such as the basal temperature, the

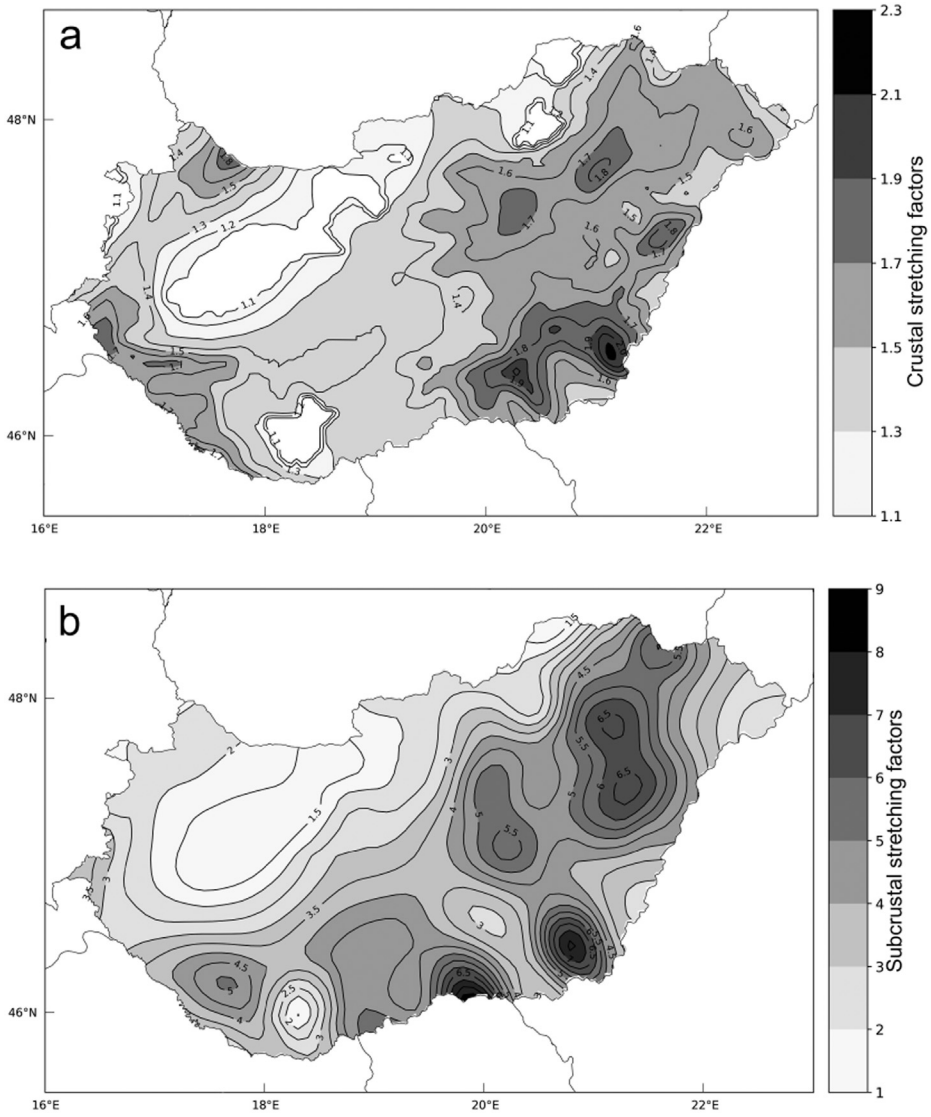


**Fig. 9.** Crustal (a) and subcrustal (b) stretching factors after Lenkey (1999).

smoother gives a direct solution. In case of non-linear problems, as for the heat generation and thermal conductivity, multiple iterations with an inflated covariance matrix of the measurement errors ($C_d$) are required to obtain the results. This procedure can be interpreted as an iterative ES, where the number of iterations has to be chosen a priori.

### 5.6. Modeling workflow

The modeling approach was to first construct a prior model with relatively low mean and median misfits with the observed temperatures, then use these results as an input for the further calculations with data assimilation, using ES-MDA. In this paper we present 3 models. The first model was constructed without data assimilation, while for the second and third model the prior parameterization is updated. The modeling workflow and the data assimilation parameters are summarized in Fig. 8 and in Table 6, respectively. All of the models run the ES-MDA with 300 realizations, incorporating 4 iterations for the multiple data assimilation. The data assimilation included varying the basal heat flow, radiogenic heat generation of the upper crust and vertical thermal conductivity of the Mesozoic carbonates and the clastic sedimentary infill. Prior uncertainties in the model parameterization were taken into account by scaling/shifting the thermal properties and boundary conditions to triangular distribution. The spatial variability of properties and boundary conditions are generated with spectral simulation, with a

**Table 3**
Overview of the boundary conditions.

| Model | Type of model | Boundary conditions used for the multi-1D calculations | | Boundary conditions used for the 3D calculations | |
|---|---|---|---|---|---|
| | | Upper | Lower | Upper | Lower |
| 1 | prior | 12 °C | Fixed heat flow value of 70 mW/m$^2$ at 10 km depth | 12 °C | Heat flow at the LAB derived from the multi-1D calculations of Model 1, 2[a] |
| 2 | posterior | | | | |
| 3 | posterior | Varying heat flow at 10 km depth calculated from the tectonic surface heat flow | | 12 °C | Heat flow at the LAB derived from the multi-1D calculations of Model 3. |

[a] Note that the multi-1D calculations of Model 1 and Model 2 are identical.

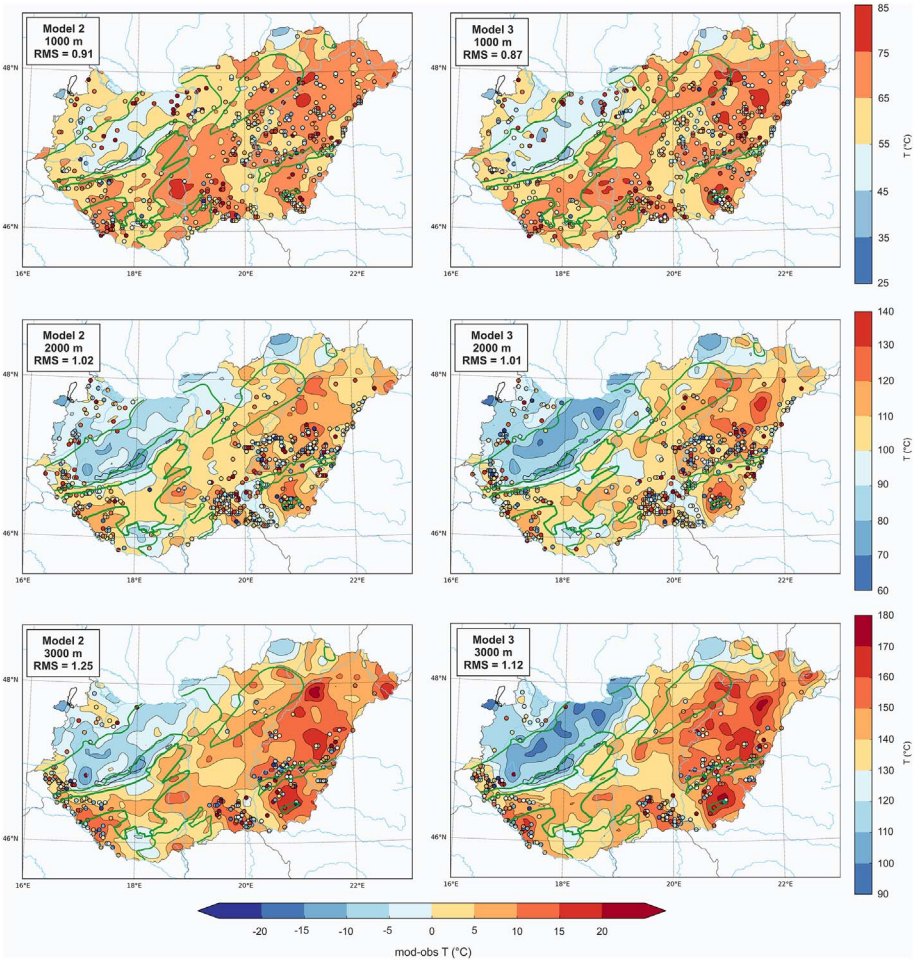


**Fig. 10.** Isodepth temperature maps of Model 2 (left) and Model 3 (right) superimposed by the misfit of the modeled and observed temperatures in ± 200m interval ($T_{mod}$–$T_{obs}$). The green contour indicates the location of the Mesozoic karstic reservoirs and their recharge areas in Hungary. The RMS misfit of every depth is indicated in the left upper corner.

spherical variogram (Yao, 2004). Variogram ranges were selected prior to the data assimilation by defining the number of cells effected by the perturbation. We varied the thermal properties through separate model runs, adopting the output of a previous model as an input for the new calculations. First the basal condition, and subsequently the shallower part of the model was updated. We prescribed larger variogram range in case of the basal heat flow, because of the small wavelength, high amplitude anomalies in the surface heat flow smooth out with increasing depth. As for the basal heat flow, we introduced shifting parameters of ± 20 mW/m$^2$. After several runs and analysis of the results, the set of parameters listed in Table 5 seemed reasonable to capture the lateral variations. The upper crustal heat production was scaled between 0.6 and 1.4 to account for the increased volumetric heat generation of dacites and rhyolites with the corresponding values of 2.2 and 2.7 μW/m$^3$ (Lenkey and Surányi, 2006), respectively. We introduced variation in the thermal conductivity of the sediments to account for potential uncertainty due to porosity-depth functions and the geometry of the layers. We allowed only a small variation in the conductivity of impermeable layers to ensure values to remain within reasonable bounds. Additionally, we tried to implicitly incorporate the thermal effect of (sub)vertical fluid transfer at recharge/discharge areas by higher than natural vertical thermal conductivity. It was performed by varying the vertical thermal conductivity of the permeable layers in a wider bandwidth (Table 6).

## 6. Results

The first and second model were calculated assuming steady-state conditions, neglecting transient geological processes. On the other hand, the thermal field in the Pannonian Basin is strongly influenced by the transient effect of recent lithospheric-scale tectonic events. To this end, the third model accounts for the thermal perturbation of recent lithospheric extension by adopting tectonic heat flow as a basal boundary condition derived from crustal and subcrustal stretching parameters.

Here we present the modeling results obtained by two different approaches. Temperature depth slices of Model 2 and Model 3 are presented between 1 and 6 km superimposed by the misfit of the modeled and observed temperatures in ± 200 m interval (Fig. 10). Model 1 is presented only by its temperature-depth profiles due to the high misfits, and, therefore unrealistic modeled temperatures. We have highlighted the areas where fractured and karstified carbonates are present. At these locations results should be treated carefully due to the influence of potential convection. Both models show a similar pattern as the surface heat flow density: in general, the models predict lower temperatures in the northwestern, and higher temperatures in the southern, eastern and southeastern part of Hungary. Modeled temperatures show a high variation in every depth interval. Some areas exhibit very high (about 200 °C) temperature at approximately 3500 m depth, forming one of the hottest regions in Europe.

The overall picture in all depth intervals suggests that the region of the Transdanubian Range is slightly colder in Model 3 than Model 2. As discussed above, low measured temperatures in this area are explained by the infiltration of cold meteoric water. Our tectonic model (Model 3) approximates the effect of downward groundwater flow with a lower error range than Model 2, but none of the models are suitable to reproduce the low measured values (note the large misfits in Fig. 10). Modeled subsurface temperatures below 3 km are not calibrated,

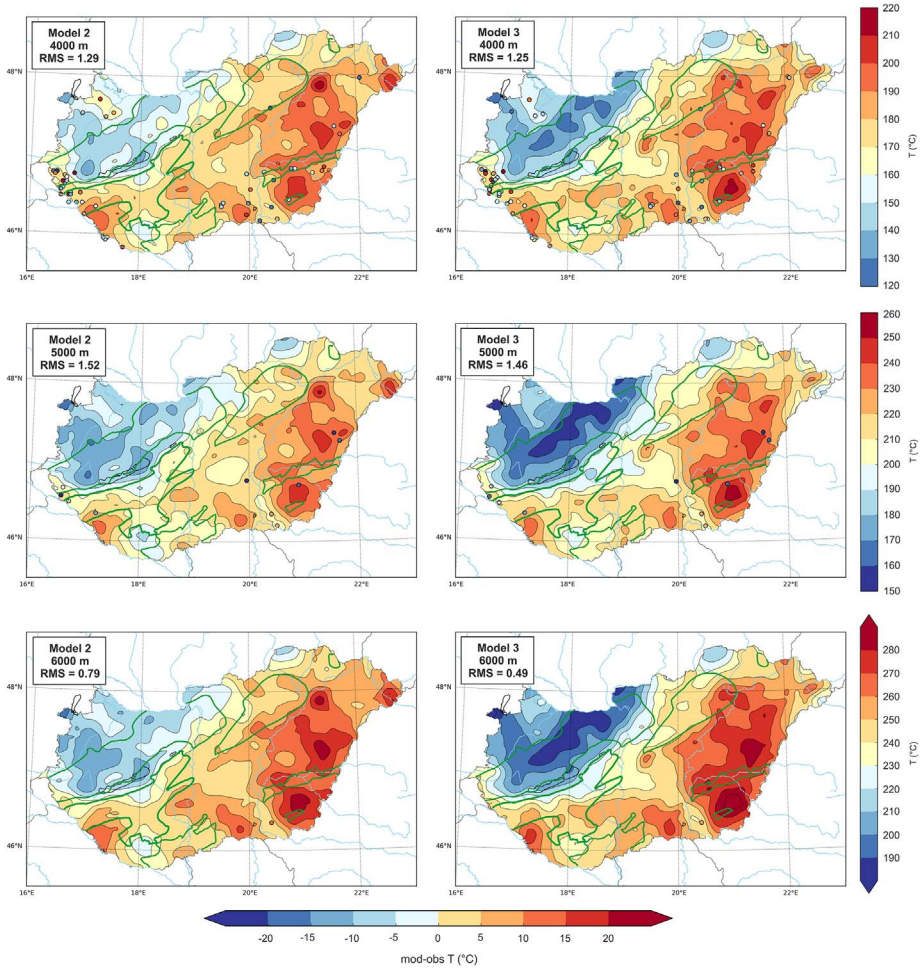


**Fig. 10.** (*continued*)

**Table 4**
Number of temperature observations used for calibration of Model 2 and Model 3.

| Model | Number of temperature observations used for calibration | | | | | | |
|---|---|---|---|---|---|---|---|
| | Total | 0–1 km | 1–2 km | 2–3 km | 3–4 km | 4–5 km | 5–6 km |
| 2 | 5135 | 2879 | 1067 | 860 | 274 | 46 | 9 |
| 3 | 3858 | 1602 | 1067 | 860 | 274 | 46 | 9 |

**Table 5**
Thermal properties used to calculate tectonic heat flow for Model 3.

| Parameter name | Value | Unit |
|---|---|---|
| Lithospheric thickness (before thinning) | 120 | [km] |
| Crustal thickness (before thinning) | 30 | [km] |
| Crustal density | 2900 | [kg/m$^3$] |
| Mantle density | 3400 | [kg/m$^3$] |
| Crustal and mantle conductivity | 3 | [W/m∗K] |
| Sediment conductivity | Adapted after Dövényi and Horváth (1988) | [W/m∗K] |
| Heat production in upper crust | variable | [mW/m$^3$] |
| Lithosphere thermal expansion | $3.2*10^{-5}$ | – |
| Thermal diffusion | $10^{-6}$ | [m/s$^2$] |
| LAB temperature | 1330 | [°C] |

because there are no reliable temperature records available. Since the temperature is calculated downwards, the conductive model is likely to underestimate the temperatures. Cooling due to groundwater downwelling is also present in some parts of the North Hungarian Range in the Northeast, reflected by both of the models. Predicted temperatures at 1 km depth in the Mecsek and Villány mountains (Fig. 1) are higher, fitting well with the high heat flow density of the area. Contrary, for deeper parts, temperatures only slightly increase.

Our models show a good fit with measured temperatures in the other parts of Transdanubia, except for a few outliers, where most likely convection due to groundwater flow occurs. The subsurface temperatures in the Danube basin are remarkably lower than in any other sub-basin in Hungary. It is in good agreement with the lower heat flow of the region compared to the other basins in Transdanubia. The warmest areas in Transdanubia can be attributed to the Drava Trough and Zala Basin, due to the blanketing effect of sediments.

In the central part of Hungary, along the River Danube, both models slightly underestimate the measured temperatures at the range of 1 to 3 km depth, where deeper records are not available. Besides the high heat flow in the area, another explanation of the relatively lower modeled temperatures can be the lack of controlling points.

Regarding the Great Hungarian Plain, the subsurface temperatures follow a slightly similar pattern as the surface heat flow at all depth levels. In general, the blanketing effect of sediments results in elevated temperatures at shallow depth. On the other hand, the sub-basins filled by more than 5 km thick sediments exhibit a relatively low heat flow, explained by the cooling effect of young sedimentation. The superposition of these two effects causes the maximum temperature to be slightly shifted towards the basement highs.

**Table 6**
Overview of the data assimilation parameters. See for the abbreviations Table 1 and Table 2.

| Model | Description | Variogram model | Variogram range in cells (1 cell ≈ 2.5 km) | Prior distribution | Scaling/shifting parameters |
|---|---|---|---|---|---|
| 2, 3 | Varying basal heat flow | Spherical | 15 | Triangular | Shift with ± 20 mW/m$^2$ |
| | Varying heat generation | | 10 | | Scale between 0.6 and 1.4 in UC |
| | Varying vertical thermal conductivity | | 10 | | Scale between 0.5 and 1.5 in Q, UP, N, M scale between 0.8 and 1.2 in LP, P |

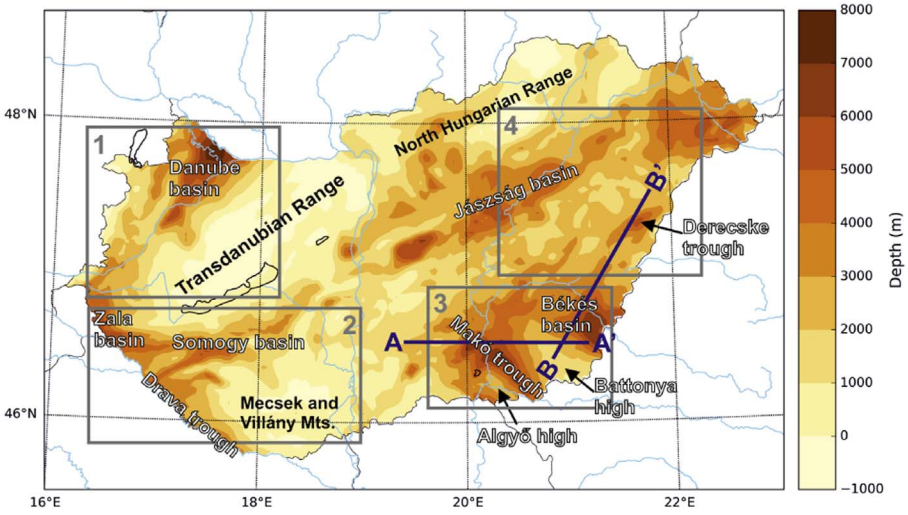


**Fig. 11.** Depth of the pre-Cenozoic basement showing the most significant sub-basins and hills of Hungary. Grey boxes indicate the location of the regions where temperature-depth profiles are available.

We have selected several wells to demonstrate the temperature-depth and thermal conductivity-depth profile of all the models (Fig. 12). Results are presented from four regions shown in Fig. 11. Region 1 represents the northwestern part of Hungary, including wells located near the Transdanubian Central Range and the Danube basin. The prior model systematically overestimates temperatures in all locations, suggesting that the model cannot account for the lower heat flow characterizing the northwestern part of Hungary. In wells Tét-5 and Szombathely-II, both Model 2 and Model 3 show a good fit with measured temperatures. Temperature records in Bősárkány-1 suggest that upwelling groundwater flow along fractured zones may be present below 4 km. On the other hand, shallower temperature records are significantly lower, which may explain that our models were not able to reproduce the potential effect of hydrothermal convection. In wells Gönyű-1 and Kehida-3, downward flow in fractured carbonatic rocks explains low measured temperatures. In Gönyű-1, Model 2 and partly Model 3 can account for the effect of downwelling by increasing the thermal conductivity of the carbonates, which forces the geothermal gradient to decrease. Contrary, neither of the models can reproduce the extremely low temperature record at ca. 3200 m depth and very high values near the surface in Kehida-3. Region 2 includes the southwestern part of Hungary, demonstrating mostly the modeling results in the Zala and Drava basins. All models fit quite well with the measured records. However, subsurface temperatures are slightly underestimated in well 2D and Nagyatád-K1. In well PAET-34, the geothermal gradient suggested by the measurements is very high, which would result in remarkably high temperatures at deeper levels. This well is located in the eastern part of the region, showing a good example of slightly underestimated temperatures in the surrounding area.

Region 3 represents the southern part of the Great Hungarian Plain, including the deepest sub-basins. It is clear that our prior model underestimates temperatures in the basement highs. On the other hand, it shows a better fit in the deep sub-basins. Model 2 and Model 3 are almost identical at all locations and predict high temperatures in the basement highs. At the same time, the deeper part of the models cannot capture adequately the very high temperature records: modeled-observed temperatures show a negative misfit in wells Alpár-I and Békés-1. Cooling due to the presence of young sediments with considerable thickness in deep troughs are quite well modeled, for instance in Makó-2. In the northern part of the Great Hungarian Plain (Region 4), the prior model is too cold at all locations, but both Model 2 and Model 3 are in good agreement with almost all of the measured records. In contrast, Sáránd-I is an exception, where the temperature-depth profiles show a misfit with an extremely high measurement. High values deep down in the basement rocks in both regions may be attributed to hydrothermal convection. The fixed thermal conductivity of the upper crust can be an explanation why our models cannot reproduce the effect of convection in the basement.

Fig. 13 shows the predicted temperatures along two profiles from the Great Hungarian Plain (for location see Fig. 11). The isotherms of the two posterior models are almost identical. The maximum deviation is ~10 °C, therefore, only Model 3 is plotted on the cross-sections. In Fig. 13a, subsurface temperatures show an eastward increasing trend towards the Battonya high, especially in the deeper part: the 300 °C isotherm is only present in the eastern part of the cross-section. In the southern part of Békés basin (Fig. 13b), the blanketing effect of sediments is clearly visible and results in only slightly elevated temperatures compared to the basement highs towards North. On the other hand, the temperature maximum is shifted towards the southern rim of the Battonya high. The temperature contrast between deep sub-basins and basement highs in Fig. 13a is more relevant: isotherms are remarkably depressed below 2 km in the Makó trough, reflecting the cooling effect of the thick sedimentary succession. The hottest region through the cross sections is linked to the Battonya high, where the modeled temperatures reach 200 °C at ca. 3500 m depth. High temperatures can be attributed to the low thermal conductivity of the very thick sedimentary cover in the surrounding sub-basins, from where heat is diverted towards the more conductive basement flank.

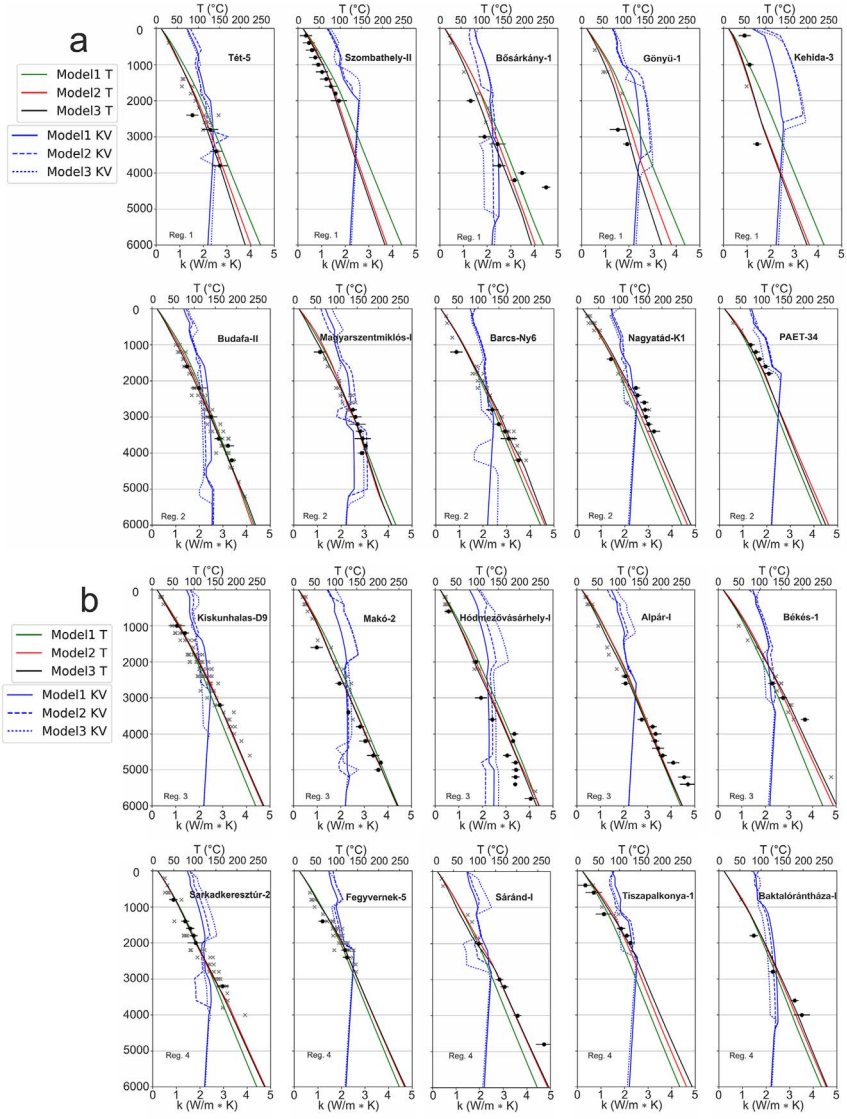


**Fig. 12.** Temperature (T)-depth and vertical thermal conductivity (KV)-depth profiles of wells located at different regions of Hungary (a: first row: Region 1, second row: Region 2; b: first row: Region 3, second row: Region 4). Measured temperatures and the corresponding uncertainties are plotted with black circles and error bars. Temperature records from wells within 10 km are indicated with grey crosses.

To outline the potential areas for EGS development, temperature at the top of the pre-Cenozoic basement is shown in Fig. 14, where the temperature values follow the same trend as the basement depth. The most promising areas are located in the Great Hungarian Plain, where an EGS project is currently in progress near Battonya (e.g. Osvald et al., 2017). Furthermore, deep geothermal exploration would also be cost-effective in the northern part of the Great Hungarian Plain.

The mean, median and Root Means Square (RMS), normalized to data error, of the misfits suggest that the overall misfit is decreasing through the data assimilation. In general, Model 1 and Model 2 (with a median of $-0.49$ and $-0.15$) slightly underestimate, and Model 3 (with a median of 0.78) slightly overestimate the measured temperatures. Although, these numbers are not entirely representative, due to the difference between the number of observations at shallow depth (in case of Model 1 and Model 2, the calibration dataset was supplemented by temperature observations calculated from the surface heat flow). For this reason, we compared the uncertainty of the three models in 1 km intervals between 1 and 6 km depth (Fig. 15), including misfits in the range of ± 500 m. Results show that all of the models overestimate temperatures at shallow depth. One explanation of the positive misfits can be that groundwater flow systems cause a net temperature reduction. This phenomena clearly exists in groundwater basins according to the numerical stimulations of Kooi (2016). Additionally, overestimated temperatures due to the uncertainty in the porosity-depth curves, or the influence of the last ice age cannot be ruled out either. Model 1 systematically underestimates the temperatures measured between 2 and 5 km depth. The mean and median misfits of the posterior models are relatively close to zero, except for the 5 km depth level with more significant negative misfits. It may be attributed to the uncertainty in the porosity-depth curves or basement depth. On the other hand, most of the negative misfits belong to wells located in the Great Hungarian Plain, where free convection of overpressured water can take place (Lenkey, 1999).

## 7. Discussion

We have established 3D lithospheric-scale temperature models for Hungary by adopting two different approaches. Subsurface temperature calculations were performed in steady-state assuming conduction as the main heat transfer mechanism. At the same time, one of our preferred models accounts for the time-dependent thermal effect of recent lithospheric extension by adapting tectonic heat flow as a basal boundary condition. Subsurface temperatures predicted by the two models are in good agreement, apart from Model 2, that predicts lower temperatures in the Transdanubian Central Range, and is slightly warmer in the Great Hungarian Plain, especially below 3 km. This deviation can be attributed to the limited area with controlling points with surface heat flow observations in case of Model 2.

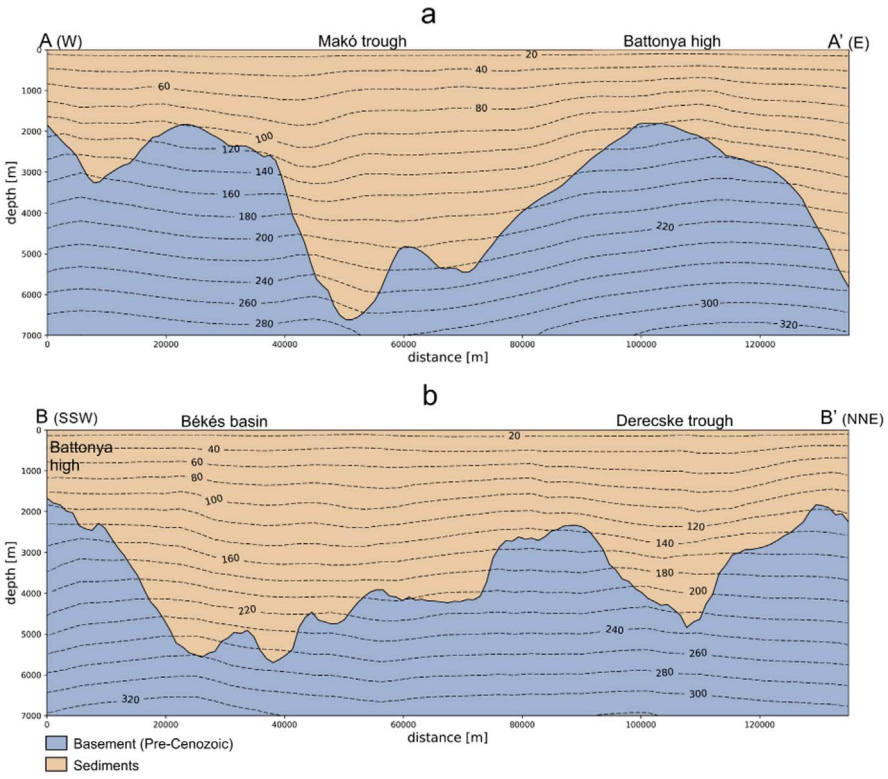


**Fig. 13.** Cross-sections from the southeastern part of Hungary (for location see Fig. 11). Subsurface temperature contours (°C) are transferred from Model 3 (dashed black lines).

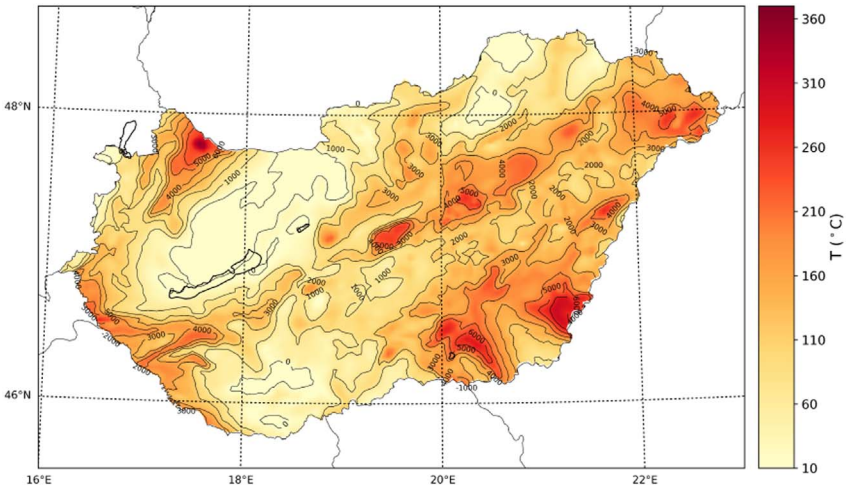


**Fig. 14.** Temperature at the top of the pre-Cenozoic basement predicted by Model 3 superimposed by the depth of the basement (m) indicated with isolines.

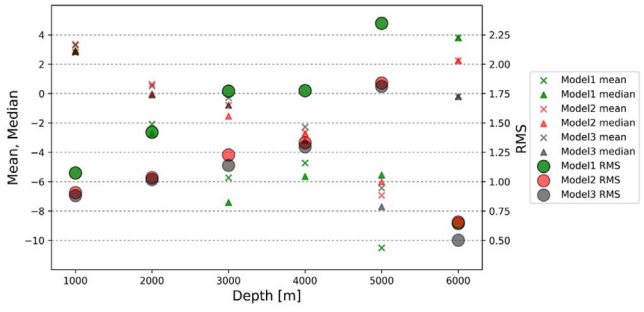


**Fig. 15.** Mean, median and RMS misfits of the three models at 1–6 km depth within a ± 500m intervals.

We first established prior models, which were updated through the data assimilation procedure to obtain a better fit with measured temperatures. Apart from changing the vertical thermal conductivity of sediments and heat generation in the upper crust, the basal boundary condition (heat flow) was also updated. Prior and posterior heat flow at 60 km depth are presented in Fig. 16. Prior heat flow in case of Model 1 and Model 2 is relatively smooth with values between 50 and 65 mW/m$^2$, corresponding to the fixed heat flow condition of 70 mW/m$^2$ at 10 km depth in the multi-1D model. Prior heat flow of Model 3 calculated from tectonic heat flow shows significant variations. In general, it follows a similar pattern as the stretching factors (Fig. 9). Posterior heat flow in both cases is lower in the deep sub-basins of the Great Hungarian Plain, especially in the Makó trough, which can be attributed to the lower surface heat flow of the area due to the cooling effect of fast sedimentation. Updated heat flow values are relatively high in the Great Hungarian Plain and near the Dráva trough and Zala basin, and lower in the northwestern part of Hungary. It is important to note that the lateral variations in posterior heat flow may not be entirely realistic, but these values provide the best fit with measured temperatures through steady-state conductive modeling. The significant difference

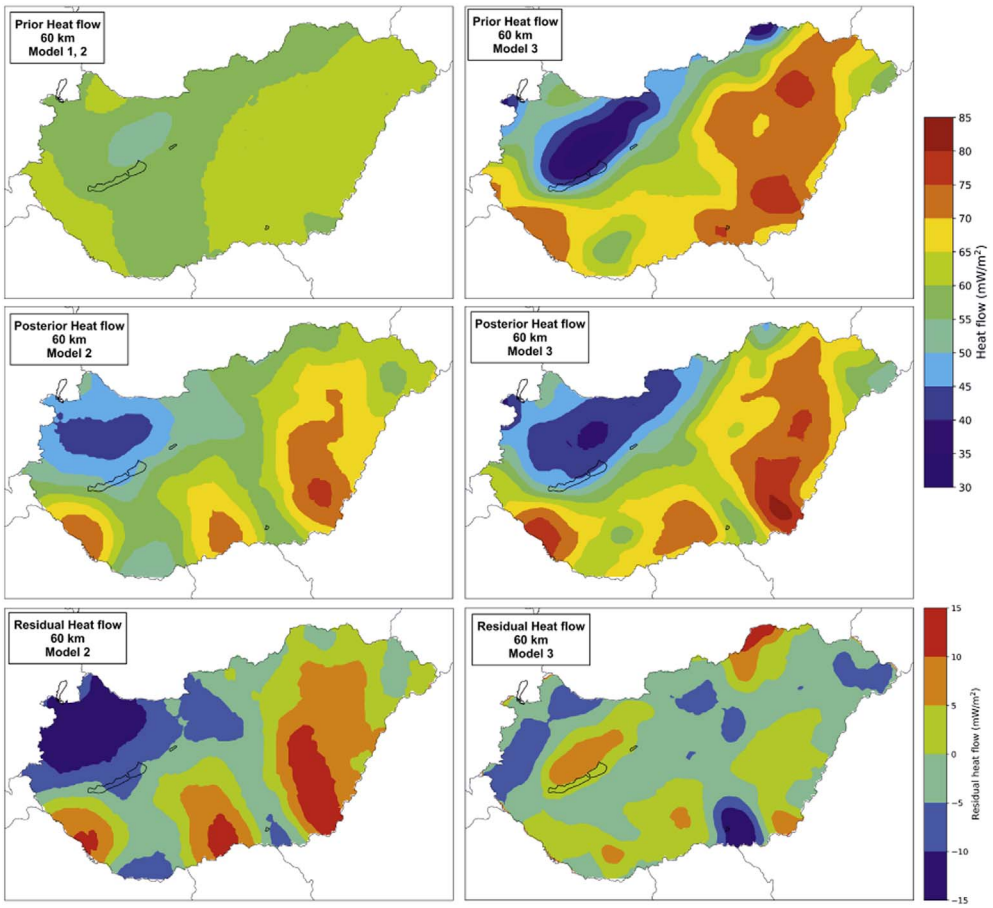


**Fig. 16.** Prior (top), posterior (middle), and residual (posterior-prior, bottom) heat flow at 60 km depth of Model 1, Model 2(left) and Model 3 (right). Note the different scale for the residual maps.

between prior and posterior heat flow, especially in case of Model 1 and Model 2 can be explained by transient effects and non-conductive heat transfer.

Our models fit well with measured temperatures, suggesting that the thermal field is predominantly conductive and is in good agreement with earlier findings of Lenkey (1999). On the other hand, convection clearly occurs at several sites in the porous sedimentary infill and fractured or karstified basement rocks. Despite the higher misfits where groundwater flows disturb the conductive regime, temperature measurements affected by fluid convection can be approximated by increasing the thermal conductivity of the corresponding layers. Regional fluid flow systems in the Pannonian Basin have the largest influence on the temperature field in the Transdanubian Range, Mecsek, Villány and Bükk mountains and their discharge areas. Therefore, the uncertainty of the models is considered higher at these locations, as temperatures in recharge and discharge areas may be overestimated and underestimated, respectively. For instance, in Kehida-3 well, only 80 °C is measured at ca. 3200 m depth, while the model predicts ca. 110 °C (Fig. 12a), meaning that the model overshoots the observed value with 30 °C. Additionally, convection due to overpressured systems can cause high negative misfits. This might be the case in Alpár-1 well with measured temperatures above 250 °C in ca 5200 m, with the corresponding misfits of −20 °C (Fig. 12b). To this end, to correct for deviations due to convective effects, a coupled modeling should be performed for the adjacent areas. Additionally, one explanation of low modeled temperatures at larger depth at Aggtelek-Gemer can be the presence of deeply infiltrating cold meteoric water, but this region is only supported by one controlling point. Therefore, our models cannot be considered reliable enough to draw this conclusion.

Prior uncertainty of the model parameters is described by triangular distribution with the variogram for spatial variation reported in Table 6. The reliability of posterior model temperatures is indicated by the misfits with measured values, described in Fig. 15. On the other hand, some regions remain uncalibrated, meaning that there is no direct measure of the misfits. Posterior uncertainties of the updated model parameters are described by the mean and standard deviation of the updated thermal properties, e.g. the basal heat flow. As the model uncertainty is set very wide and the observation error rather narrow, the variation of posterior values are also narrow, resulting in low posterior uncertainties. Standard deviation of modeled temperature varies after each data assimilation step (depending on the varied thermal property). After each modeling step, standard deviation values remain below 10 °C in the top 6 km, which therefore can be considered as the general reliability of the models. Additionally, the degrees of freedom in the model parameters is much larger than the number of calibration data points, meaning that the inverse problem is underdetermined. Therefore, model solutions are non-unique and the modeled temperatures of uncalibrated regions are considered ambiguous.

We have compared our results with the isodepth temperature maps based on the interpolation of measured temperatures after Dövényi et al. (2005). These maps are only available in 1 and 2 km depth, but our posterior models conform well with them, especially where controlling points are present and the thermal field is dominantly conductive. Moreover, Model 3 predicts similar subsurface temperatures in the western part of Hungary to the time dependent lithospheric-scale thermal model (of the Alpine-Pannonian transition zone) of Lenkey et al. (2017). Extremely elevated temperatures modeled in the Great Hungarian Plain are in agreement with the high heat flow related to the asthenospheric dome below the area (Horváth et al., 2015). Additionally, local reduction of the heat flow in the sub-basins due to thick, young sediments (Lenkey et al., 2002) is also reflected by the modeled temperature field. Modeled Moho temperatures in the most

extended part of the Pannonian Basin reach even 850 °C (Appendix 1), which is significantly higher than previous results of Tesauro et al. (2009). This is fundamentally due to the different lithospheric thickness used for modeling. On the other hand, the peripheral parts of the basin exhibit lower modeled temperature at the Moho (around 700 °C).

In theory, it is possible to reach even lower misfits by decreasing the variogram sizes and/or applying a wider range for the scaling/shifting parameters of the thermal properties, but high-amplitude local variations in these properties may be unrealistic. Therefore, data assimilation parameters of the thermal properties should be selected carefully: variation and spatial correlation lengths should be introduced within reasonable bounds.

## 8. Conclusions

In this paper we have presented a new lithospheric-scale 3D temperature model of Hungary. The most important innovation of the applied method is that the thermal properties of the layers are updated through the ensemble smoother with multiple data assimilation technique. Our model is capable to account for observed thermal anomalies due to potential variations in the lithospheric thickness and processes in the underlying mantle by laterally varying the basal heat flow boundary condition. Temperature-depth profiles and the uncertainties clearly support the added value of the data assimilation: our posterior models show considerably better fit with measured records than the prior model. The updated models approximate temperature measurements disturbed by fluid convection by modifying the thermal conductivity of the layers. On the other hand, results should be treated carefully in recharge and discharge areas connected to gravity-driven fluid flows and in the overpressured domain, and also in regions with lack of controlling points. Our models are able to reproduce the thermal effect of lithospheric extension and sediment infill of the Pannonian Basin. Furthermore, the variation in the onset and rate of sedimentation between the northwestern and southeastern part of Hungary is also mirrored in the subsurface temperatures. In spite of the sediment blanketing, results suggest that the hottest areas below 3 km are linked to the basement highs surrounded by deep sub-basins of the Great Hungarian plain. Subsurface temperatures predicted by the two different models are in good agreement, suggesting the stability of the solution. Therefore, it appears that our models are capable to describe the subsurface temperature distribution in the whole lithosphere. Furthermore, our models reveal potential target areas for deep geothermal development and can serve as an input for geothermal resource assessment. Future models may further be refined by having better constraints on the depth of the basement and the geometry and thermal properties of the sedimentary layers. The method can also be used for smaller-scale models, in order to predict the temperature distribution at a specific site.

Supplementary data to this article can be found online at https://doi.org/10.1016/j.gloplacha.2017.09.020.

## Acknowledgements

The research leading to these results has received funding from the European Union's Seventh Framework Programme under grant agreement no. 608553 Project IMAGE. We thank the reviewers for the very constructive reviews.

## References

Bada, G., et al., 2007. Present-day stress field and tectonic inversion in the Pannonian basin. Glob. Planet. Chang. 58 (1), 165–180.
Balázs, A., Matenco, L., Magyar, I., Horváth, F., Cloetingh, S., 2016. The link between tectonics and sedimentation in back-arc basins: new genetic constraints from the analysis of the Pannonian Basin. Tectonics 35 (6), 1526–1559.
Balázs, A., et al., 2017. Symmetry during the syn-and post-rift evolution of extensional back-arc basins: the role of inherited orogenic structures. Earth Planet. Sci. Lett. 462, 86–98.
Báldi, T., Royden, L.H., 1986. Mid-Tertiary Stratigraphy and Paleogeographic Evolution of Hungary. Akadémiai Kiadó.
Balla, Z., 1986. Palaeotectonic reconstruction of the central Alpine-Mediterranean belt for the Neogene. Tectonophysics 127 (3), 213–243.
Balla, Z., 1988. Clockwise paleomagnetic rotations in the Alps in the light of the structural pattern of the Transdanubian Range (Hungary). Tectonophysics 145 (3–4), 277–292.
Berczi, I., 1988. Preliminary Sedimentological Investigation of a Neogene Depression in the Great Hungarian Plain. (Chapter 10).
Bonté, D., Van Wees, J.-D., Verweij, J., 2012. Subsurface temperature of the onshore Netherlands: new temperature dataset and modelling. Neth. J. Geosci. 91 (4), 491–515.
Čermák, V., Bodri, L., 1986. Two-dimensional temperature modelling along five East-European geotraverses. J. Geodyn. 5 (2), 133–163.
Chapman, D., 1986. Thermal gradients in the continental crust. Geol. Soc. Lond., Spec. Publ. 24 (1), 63–70.
Cloetingh, S., et al., 2010. Lithosphere tectonics and thermo-mechanical properties: an integrated modelling approach for Enhanced Geothermal Systems exploration in Europe. Earth Sci. Rev. 102 (3), 159–206.
Csontos, L., Nagymarosy, A., 1998. The Mid-Hungarian line: a zone of repeated tectonic inversions. Tectonophysics 297 (1), 51–71.
Csontos, L., Vörös, A., 2004. Mesozoic plate tectonic reconstruction of the Carpathian region. Palaeogeogr. Palaeoclimatol. Palaeoecol. 210 (1), 1–56.
Dövényi, P., Horváth, F., 1988. A review of temperature, thermal conductivity, and heat flow Data for the Pannonian Basin. In: Horvath, F., Royden, L.H. (Eds.), The Pannonian Basin. 45. Am. Assoc. Petrol. Geol. Memoir, pp. 195–233.
Dövényi, P., Horváth, F., Drahos, D., 2002. Geothermal Thermic Map (Hungary). Atlas of Geothermal Resources in Europe. pp. 267 (Publ. No. EUR, 17811).
Dövényi, P., Homola, V., Horváth, F., Kohl, T., Rybach, L., 2005. European HDR/EGS Resources: Future Potential Development in Hungary. (Order(G109/05), 22.13).
Emerick, A.A., Reynolds, A.C., 2013. Ensemble smoother with multiple data assimilation. Comput. Geosci. 55, 3–15.
Faccenna, C., et al., 2014. Mantle dynamics in the Mediterranean. Rev. Geophys. 52 (3), 283–332.
Fodor, L., et al., 2005. An outline of neotectonic structures and morphotectonics of the western and central Pannonian Basin. Tectonophysics 410 (1), 15–41.
Fodor, L.I., et al., 2008. Miocene emplacement and rapid cooling of the Pohorije pluton at the Alpine-Pannonian-Dinaridic junction, Slovenia, Orogenic Processes in the Alpine Collision Zone. Springer, pp. S255–S271.
Fokker, P., Wassing, B., van Leijen, F., Hanssen, R., Nieuwland, D., 2016. Application of an ensemble smoother with multiple data assimilation to the Bergermeer gas field, using PS-InSAR. Geomech. Energy Environ. 5, 16–28.
Goldscheider, N., Mádl-Szőnyi, J., Erőss, A., Schill, E., 2010. Review: thermal water resources in carbonate rock aquifers. Hydrogeol. J. 18 (6), 1303–1318.
Gordon, D., Flemings, P., 1998. Generation of Overpressure and Compaction-driven Fluid Flow in a Plio-Pleistocene Growth-Faulted Basin, Eugene Island. 330. pp. 177–196.
Goutorbe, B., Lucazeau, F., Bonneville, A., 2007. Comparison of several BHT correction methods: a case study on an Australian data set. Geophys. J. Int. 170 (2), 913–922.
Haas, J., Budai, T., Csontos, L., Fodor, L., Konrád, G., 2010. Pre-Cenozoic Geological Map of Hungary, 1:500 000. Geological Institute of Hungary, Budapest.
Hámor, G., 2001. Genesis and evolution of the Pannonian Basin. In: Geology of Hungary. Eötvös Univ. Press, Budapest, pp. 193–265.
Hantschel, T., Kauerauf, A.I., 2009. Fundamentals of Basin and Petroleum Systems Modeling. Springer Science & Business Media.
Harangi, S., Lenkey, L., 2007. Genesis of the Neogene to Quaternary volcanism in the Carpathian-Pannonian region: role of subduction, extension, and mantle plume. Geol. Soc. Am. Spec. Pap. 418, 67–92.
Hasterok, D., Chapman, D., 2011. Heat production and geotherms for the continental lithosphere. Earth Planet. Sci. Lett. 307 (1), 59–70.
Hofmann, T., Schönlaub, H.P., 2007. Geo-Atlas Österreich: die Vielfalt des geologischen Untergrundes. Böhlau Verlag Wien.
Horváth, F., 1993. Towards a mechanical model for the formation of the Pannonian basin. Tectonophysics 226 (1), 333–357.
Horváth, F., Cloetingh, S., 1996. Stress-induced late-stage subsidence anomalies in the Pannonian basin. Tectonophysics 266 (1–4), 287–300.
Horváth, F., Rumpler, J., 1984. The Pannonian basement. Acta Geol. Hung. 27 (3–4), 229–235.
Horváth, F., et al., 2006. Formation and deformation of the Pannonian Basin: constraints from observational data. Geol. Soc. Lond. Mem. 32 (1), 191–206.
Horváth, F., et al., 2015. Evolution of the Pannonian basin and its geothermal resources. Geothermics 53, 328–352.
Juhász, G., 1991. Lithostratigraphical and sedimentological framework of the Pannonian (sl) sedimentary sequence in the Hungarian Plain (Alföld), Eastern Hungary. Acta Geol. Hung. 34 (1–2), 53–72.
Karátson, D., et al., 2013. Morphometrical and geochronological constraints on the youngest eruptive activity in East-Central Europe at the Ciomadul (Csomád) lava dome complex, East Carpathians. J. Volcanol. Geotherm. Res. 255, 43–56.
Kooi, H., 2016. Groundwater flow as a cooling agent of the continental lithosphere. Nat. Geosci. 9 (3), 227.
Kovács, I., Zajacz, Z., Szabó, C., 2004. Type-II xenoliths and related metasomatism from the Nógrád-Gömör Volcanic Field, Carpathian-Pannonian region (northern Hungary–southern Slovakia). Tectonophysics 393 (1), 139–161.
Lankreijer, A., Bielik, M., Cloetingh, S., Majcin, D., 1999. Rheology predictions across the western Carpathians, Bohemian massif, and the Pannonian basin: implications for tectonic scenarios. Tectonics 18 (6), 1139–1153.
Lenkey, L., 1999. Geothermics of the Pannonian Basin and its Bearing on the Tectonics of

Basin Evolution. PhD thesis. Vrije Universiteit, Amsterdam, pp. 215.
Lenkey, L., Surányi, G., 2006. Study of the heat production of Neogene volcanic rocks from Hungary (in Hungarian). Magyar Geofizika 47 (/4).
Lenkey, L., Dövényi, P., Horváth, F., Cloetingh, S., 2002. Geothermics of the Pannonian Basin and its Bearing on the Neotectonics. EGU Stephan Mueller Special Publication Series 3. pp. 29–40.
Lenkey, L., et al., 2017. Lithospheric scale 3D thermal model of the Alpine–Pannonian transition zone. Acta Geodyn. Geomater. 1–22.
Limberger, J., et al., 2014. Assessing the prospective resource base for enhanced geothermal systems in Europe. Geothermal Energy. Science 2 (1), 55.
Limberger, J., et al., 2017. A public domain model for 1D temperature and rheology construction in basement-sedimentary geothermal exploration: an application to the Spanish Central System and adjacent basins. Acta Geodaet. Geophys. 1–14.
Mádl-Szőnyi, J., Tóth, J., 2009. A hydrogeological type section for the Duna-Tisza Interfluve, Hungary. Hydrogeol. J. 17 (4), 961–980.
Mádl-Szőnyi, J., et al., 2017. Confined carbonates–Regional scale hydraulic interaction or isolation? In: Marine and Petroleum Geology.
Magyar, I., Sztanó, O., 2008. Is there a Messinian unconformity in the Central Paratethys. Stratigraphy 5 (3–4), 245–255.
Magyar, I., Geary, D.H., Müller, P., 1999. Paleogeographic evolution of the Late Miocene Lake Pannon in Central Europe. Palaeogeogr. Palaeoclimatol. Palaeoecol. 147 (3), 151–167.
Magyar, I., et al., 2013. Progradation of the paleo-Danube shelf margin across the Pannonian Basin during the Late Miocene and Early Pliocene. Glob. Planet. Chang. 103, 168–173.
Márton, E., Fodor, L., 2003. Tertiary paleomagnetic results and structural analysis from the Transdanubian Range (Hungary): rotational disintegration of the Alcapa unit. Tectonophysics 363 (3), 201–224.
Matenco, L., Radivojević, D., 2012. On the formation and evolution of the Pannonian Basin: constraints derived from the structure of the junction area between the Carpathians and Dinarides. Tectonics 31 (6).
Matenco, L., et al., 2016. The interplay between tectonics, sediment dynamics and gateways evolution in the Danube system from the Pannonian Basin to the western Black Sea. Sci. Total Environ. 543, 807–827.
Merten, S., Matenco, L., Foeken, J., Stuart, F., Andriessen, P., 2010. From nappe stacking to out-of-sequence postcollisional deformations: Cretaceous to Quaternary exhumation history of the SE Carpathians assessed by low-temperature thermochronology. Tectonics 29 (3).
Nagymarosy, A., Muller, P., 1988. Some aspects of Neogene biostratigraphy in the Pannonian Basin. In: Horvath, F., Royden, L.H. (Eds.), The Pannonian Basin. Am. Assoc. Petrol. Geol. Memoir (Chapter 6).
Osvald, M., Szanyi, J., Medgyes, T., Kóbor, B., Csanádi, A., 2017. Geothermal energy developments in the district heating of Szeged. Eur. Geologist Eur. Geologist 30.
Pavelić, D., Avanić, R., Bakrač, K., Vrsaljko, D., 2001. Early Miocene braided river and lacustrine sedimentation in the Kalnik mountain area (Pannonian Basin System, NW Croatia). Geol. Carpath. 52 (6), 375–386.
Piller, W.E., Harzhauser, M., Mandic, O., 2007. Miocene Central Paratethys stratigraphy–current status and future directions. Stratigraphy 4.
Pogácsás, G., et al., 1988. Seismic facies, electro facies and Neogene sequence chronology of the Pannonian Basin. Acta Geol. Hung. 31 (3–4), 175–207.
Pollack, H.N., Chapman, D.S., 1977. On the regional variation of heat flow, geotherms, and lithospheric thickness. Tectonophysics 38 (3-4), 279–296.
Ratschbacher, L., Frisch, W., Linzer, H.G., Merle, O., 1991. Lateral extrusion in the Eastern Alps, part 2: structural analysis. Tectonics 10 (2), 257–271.
Ravnik, D., Rajver, D., Poljak, M., Živčić, M., 1995. Overview of the geothermal field of Slovenia in the area between the Alps, the Dinarides and the Pannonian basin. Tectonophysics 250 (1–3), 135–149.
Rezessy, G., Szanyi, J., Hámor, T., 2005. Report on Development of Geothermal Energy Inventory (in Hungarian). 82 Hungarian Geological Survey, Budapest.
Rotár-Szalkai, Á., et al., 2017. Outline and joint characterization of Transboundary geothermal reservoirs at the western part of the Pannonian basin. Geothermics 70, 1–16.
Royden, L., Keen, C., 1980. Rifting process and thermal evolution of the continental margin of eastern Canada determined from subsidence curves. Earth Planet. Sci. Lett. 51 (2), 343–361.
Royden, L., Horváth, F., Rumpler, J., 1983. Evolution of the Pannonian Basin System: 1. Tectonics. Tectonics 2 (1), 63–90.
Schatz, J.F., Simmons, G., 1972. Thermal conductivity of earth materials at high temperatures. J. Geophys. Res. 77 (35), 6966–6983.
Schmid, S.M., et al., 2008. The Alpine-Carpathian-Dinaridic orogenic system: correlation and evolution of tectonic units. Swiss J. Geosci. 101 (1), 139–183.
Sclater, J., et al., 1980. The formation of the intra-Carpathian basins as determined from subsidence data. Earth Planet. Sci. Lett. 51 (1), 139–162.
Szabó, C., Harangi, S., Csontos, L., 1992. Review of Neogene and Quaternary volcanism of the Carpathian-Pannonian region. Tectonophysics 208 (1–3), 243–256.
Tari, G., Horváth, F., Rumpler, J., 1992. Styles of extension in the Pannonian Basin. Tectonophysics 208 (1–3), 203–219.
Tari, G., et al., 1999. Lithospheric structure of the Pannonian basin derived from seismic, gravity and geothermal data. Geol. Soc. Lond., Spec. Publ. 156 (1), 215–250.
Tesauro, M., Kaban, M.K., Cloetingh, S.A., 2009. A new thermal and rheological model of the European lithosphere. Tectonophysics 476 (3), 478–495.
Theissen, S., Rüpke, L., 2010. Feedbacks of sedimentation on crustal heat flow: new insights from the Vøring Basin, Norwegian Sea. Basin Res. 22 (6), 976–990.
Tiliţă, M., Matenco, L., Dinu, C., Ionescu, L., Cloetingh, S., 2013. Understanding the kinematic evolution and genesis of a back-arc continental “sag” basin: the Neogene evolution of the Transylvanian Basin. Tectonophysics 602, 237–258.
Tóth, J., Almási, I., 2001. Interpretation of observed fluid potential patterns in a deep sedimentary basin under tectonic compression: Hungarian Great Plain, Pannonian Basin. Geofluids 1 (1), 11–36.
Tóth, G., et al., 2016. Transboundary fresh and thermal groundwater flows in the west part of the Pannonian Basin. Renew. Sust. Energ. Rev. 57, 439–454.
Ustaszewski, K., et al., 2010. Evolution of the Adria-Europe plate boundary in the northern Dinarides: From continent-continent collision to back-arc extension. Tectonics 29 (6).
Vakarcs, G., et al., 1994. Third-order Middle Miocene-Early Pliocene depositional sequences in the prograding delta complex of the Pannonian Basin. Tectonophysics 240 (1–4), 81–106.
Van Wees, J., et al., 2009. Probabilistic tectonic heat flow modeling for basin maturation: assessment method and applications. Mar. Pet. Geol. 26 (4), 536–551.
Xu, Y., et al., 2004. Thermal diffusivity and conductivity of olivine, wadsleyite and ringwoodite to 20 GPa and 1373 K. Phys. Earth Planet. Inter. 143, 321–336.
Yao, T., 2004. Reproduction of the mean, variance, and variogram model in spectral simulation. Math. Geol. 36 (4), 487–506.